PERGAMON

Computers & Fluids 30 (2001) 1–35

computers & fluids

www.elsevier.com/locate/compfluid

Sensitivity of turbulent shedding flows to non-linear stress–strain relations and Reynolds stress models

D. Lakehal[a,*], F. Thiele[b]

[a]*Institute of Energy Technology, Nuclear Engineering Laboratory, ETH-Zentrum/CLT, 8092 Zürich, Switzerland*
[b]*Hermann Föttinger Institut für Strömungsmechanik, Technische Universität Berlin, Müller-Breslau Strasse 8, D-10623, Berlin, Germany*

Received 9 November 1999; received in revised form 29 November 1999; accepted 2 December 1999

Abstract

The efficiency of various modelling strategies based on the non-linear representation of Reynolds stress in terms of strain and vorticity rates, is addressed for vortex-shedding flows past a bluff body. Two of these models were successfully modified to cope with highly-strained flows. Further, a novel modelling methodology is proposed, based on zonal coupling of a second-order closure for turbulence, solving the outer core flow region, with a one-equation non-linear model for near-wall flow regions. The merits of each approach are evaluated through comparison of the results with the available experimental data for vortex-shedding flow past a square cylinder at $Re = 22{,}000$. All the models were found to reproduce fairly well the shedding dynamics, with a common predictive trend; that is, the total fluctuating energy is in good accord with the measurements whereas the turbulent kinetic energy is significantly underestimated. The stress–strain relationships were found to be more dominant with incorporating the cubic stress–strain products forming the anisotropic stress tensor. The novel zonal second-order closure was found to be superior to all other methods. The method was also capable to predict the periodic doubling phenomenon, in accord with direct numerical simulation (DNS) and experiments in which the flow was deliberately forced to two-dimensionality.

* Corresponding author. Tel.: +41-1-632-4613; fax: +41-1-632-1166.
E-mail addresses: lakehal@iet.mavt.ethz.ch (D. Lakehal), thiele@pi.tu-berlin.de (F. Thiele).

0045-7930/01/$ - see front matter
PII: S0045-7930(00)00003-7

1. Introduction

Complex flows involving transient, turbulent reaction, with relevance to practical applications are currently appealing for reliable numerical simulation to enhance our understanding of the underlying physical mechanisms. A recurrent practice in industrial applications is the triggering of fluid-engineering devices, for example, the use of a bluff body for flame stabilization in combustion chambers where the coherent structures play a key role in the mixing process. With regard to this latter aspect, the result can exhibit strong similarities to external, vortex-shedding flows past single obstacles, an area which has been a major attraction for many specialists in wind engineering. Nonetheless, in such flows, turbulence plays a major role and its accurate representation is crucial for correct prediction. This can be achieved by considering the effects of the whole spectrum of turbulent scales on the mean flow, a possibilty reserved to direct numerical simulation (DNS). The large eddy simulation (LES) concept seems to be a very promising route for approaching complex flows, though it does not yet reveal a coherent picture in tackling a certain category of complex flows, such as those featuring wave motion. From purely computational considerations these two sophisticated prediction tools are currently confined to low Reynolds number flows. Otherwise, one is forced to retain the method based on the solution of the *Reynolds Averaged Navier–Stokes Equations* (RANS), combined with statistical turbulence models, at least for the foreseeable future. Beyond the fact that, from a physical standpoint, two-equation closure modelling is an acceptable level of closure, if properly employed so as to capture the basic mechanisms related to turbulence, it actually constitutes an attractive and viable alternative for its practical advantages. A pure Reynolds stress model (RSM) which, by concept, constitutes the highest level of closure, is naturally preferred but, due to its severe complications, many users are simply discouraged to use it, in particular, for complex flows where, in addition, direct integration to solid walls via a low-Re scheme is needed.

In the case of turbulent flows with organized wave motion, such as the well-documented flow past a slender, square cylinder — the presently studied test case — the efficacy of both two-equation and second-order closures can be adequately assessed through the comparison of integral parameters, namely the lift and drag coefficients (C_l and C_d), and the Strouhal number ($St = f_s D/U$, where f_s is the frequency of shedding, D the diameter, and U the freestream velocity). Experiments show that this flow is basically two-dimensional in the mean, and has a transitional behaviour which takes place at the cylinder side walls.

The present work aims at completing a major undertaking whose primary objective was to scrutinize all the possible simulation issues for vortex-shedding flows past circular, square and triangular cylinders. The completed parts refer to the contributions that addressed the impact of numerical approach [1], together with a critical comparison of the RANS and LES predictive capabilities for these flows [2]. With the present contribution, we try to shed light on the efficacy and behaviour of more sophisticated closures for turbulence than the conventional eddy-viscosity models, namely a selected set of well-established, explicit algebraic stress models (EASMs), along with a novel strategy based on zonal coupling of a RSM solution for the outer core flow region and a one-equation EASM for near-wall regions. The selected algebraic models are derived from different strategies and range up to cubic functional formulations of the Reynolds stress in terms of strain and vorticity-rate tensors. Two of these models were

significantly modified with the objective of making them capable of handling highly strained flows. The calculations were performed using the finite-volume computer program (ELAN2D) developed at the University of Berlin [1]. The results are compared with the measurements of Lyn et al. [3] and Durao et al. [4].

2. Some previous attempts

A large number of approaches for modelling such flows can be reported today, with the employed turbulence models ranging up to the most sophisticated one, that is the costly second-order closure strategy. The conclusions that have been drawn so far can be summarized as follows: Linear eddy-viscosity models (EVM) with wall functions, without resorting to any kind of ad-hoc model correction, are unlikely to predict shedding due to the excessive damping that is introduced through the spurious production of turbulence in stagnation flow regions, and also due to near-wall treatments bridging the semi-viscous sublayer. An exception is the work of Bosch [5], who recalculated the flow with different inflow conditions of turbulence than had been used previously [6] and argued that an imposed turbulence length-scale of $L_u/D = 0.1$ was more realistic than the 1.0 scale used hitherto. The shedding motion was found to really persist only by direct integration to the semi-viscous sublayer, using either a near-wall one-equation model [6,5] or a pure low-*Re* model [7]. Deng et al. [8] used a simple Baldwin–Lomax model for the computation of this flow, and surprisingly obtained better results than with a two-equation turbulence model. Though all these latter strategies have indeed shown noticeable improvement in predicting global forces, they have a common defect: that is, the time-averaged turbulent kinetic energy is significantly underestimated, except for Deng et al. whose method does not predict this quantity, and the periodic kinetic energy is never recovered. From previous works, it appears that the inaccurate representation of the non-coherent fluctuations may be attributed to the two-dimensional idealization, which neglects one turbulent fluctuating component, though the mean flow is actually quasi two-dimensional. This issue is discussed here too.

Reducing the excessive turbulence production at impingement, either by means of ad-hoc measures, such as the Kato and Launder's [9] modification, or by suppressing it explicitly, was partially successful: for instance, the drag coefficient ($\bar{C}_d$) was well predicted at the expense of a grossly overpredicted recirculation zone. Recourse to Reynolds Stress models yielded the best agreement in terms of integral forces, but overpredicted the periodic fluctuating energy [6].

A close look at the attempts reported above, and to those of many others, reveal that the conditions of application of the various modelling strategies are not consistent with regard to the imposed conditions of turbulence at inflow, in particular, the rate of dissipation ε. This point is also discussed here. LES of this flow has been performed on both two-dimensional and three-dimensional computational grids by Murakami et al. [10], and has been reported in the *Workshop on LES of Flows past Bluff Bodies* [11]. Recent LES results have been presented by Yu and Kareem [12] and Lakehal et al. [2] as well. On the basis of the different results, actually of a very mixed quality, it seems that the superiority of the LES approach cannot yet be fully acknowledged. A common feature to most of the contributors was that the LES results

can be severely degraded if accurate numerical discretization schemes and sufficient computational resources are not guaranteed to reach full statistical steadiness. In contrast to 2D-RANS, one should recognize that LES (which is 3D) predicts correctly the non-coherent fluctuations, though there is no evidence that the coherent fluctuations have been to date correctly predicted.[1]

3. Ensemble-averaged flow equations

Considering incompressible, turbulent motion of a Newtonian, viscous fluid, the velocity field u_i and kinematic pressure p are obtained by solving the mass conservation and Navier–Stokes equations which read

$$\frac{\partial u_i}{\partial x_i} = 0; \quad \text{and} \quad \frac{\mathrm{D}u_i}{\mathrm{D}t} = -\frac{\partial p}{\partial x_i} + \nu \nabla^2 u_i \tag{1}$$

respectively, where $\mathrm{D}/\mathrm{D}t = \partial/\partial t + u_j \partial/\partial x_j$ denotes the mean convective derivative. In the decomposition procedure of the fluctuating signal representing a turbulent flow with periodic unsteadiness proposed by Reynolds and Hussein [13], a flow variable (f) is decomposed according to

$$f = \bar{f} + \tilde{f} + f' \quad \text{and} \quad \langle f \rangle = \bar{f} + \tilde{f} \tag{2}$$

where $\tilde{f}$ denotes the alternate wave and f' the superimposed turbulent or non-coherent fluctuations. The phase- or *ensemble-average* is represented by the quantity $\langle f \rangle$, which reduces to $\bar{f}$ in steady-state. Note that this decomposition is valid for high Reynolds number flows in which the stochastic, three-dimensional fluctuations, of very small scales only, are superimposed on the periodic motion, be it two-dimensional or three-dimensional. The phase-averaged mass and momentum conservation equations representing the mean wave flow are obtained by applying the decomposition (2) to the system of equations (1). The resulting system of *Phase-Averaged Navier–Stokes* equations takes the following form:

$$\frac{\partial \langle u_i \rangle}{\partial x_i} = 0; \qquad \frac{\mathrm{D}\langle u_i \rangle}{\mathrm{D}t} = -\frac{\partial \langle p \rangle}{\partial x_i} + \nu \nabla^2 \langle u_i \rangle - \frac{\partial \langle \tau_{ij} \rangle}{\partial x_j} \tag{3}$$

in which, by virtue of the general property $\overline{\tilde{f}g'} = 0$:

$$\overline{\langle \tau_{ij} \rangle} = \langle \overline{u_i' u_j'} \rangle = \overline{u_i' u_j'} + \overline{\tilde{u}_i \tilde{u}_j} \tag{4}$$

Clearly, this system of equations is closed provided the phase-averaged Reynolds stress tensor ($\langle u_i' u_j' \rangle$) is modelled appropriately. In fact, it is the Reynolds stress tensor ($u_i' u_j'$), which here represents the cross-correlations of the superimposed velocity fluctuations, which really needs a

[1] This quantity has never been compared in any of the LES contributions.

closure law, since the wave-induced Reynolds stress tensor ($\tilde{u}_i\tilde{u}_j$) is implicitly contained in $\langle u_i' u_j' \rangle$. However, the simulation of an inherently-turbulent shedding flow by invoking the classical Reynolds averaging (i.e. $\tilde{f} = 0$), in steady-state, will ignore the effects of the wave-induced stress $\overline{\tilde{u}_i\tilde{u}_j}$ (Eq. (4)) in the momentum transport equations unless an additional model for these periodic fluctuations is incorporated. In such cases, the calculation leads to misrepresentation of the rate of momentum exchange in the wake, with major consequences on the flow solution. Conceptually, the phase-averaged Navier–Stokes approach is meaningful providing the flow is of a wavy nature. Therefore, it is probably suitable to refer to this category of modelling strategy by *Conditional Phase-Averaged Navier–Stokes Equations*, rather than by RANS.

At this stage, it appears necessary to recall some of the restrictions to the modelling approach for vortex-shedding flows dominated by a single shedding frequency. First, two-equation modelling strategies invoke the assumption of a unique turbulent length-scale, or universal turbulence spectrum, and are hence valid only for turbulent flows in which the non-coherent fluctuations evolve within high frequency spectral range (small scales). Furthermore, global averaging of turbulent structures over all scales, requires the dominating shedding-frequency to fall within the spectral range where it does not lead to significant interactions with the spectrum of the modelled non-coherent fluctuations. These principles should require the imposed turbulent length-scale to be smaller than the body itself.

4. Turbulence closure

In the context of two-equation turbulence modelling, in which the local state of turbulence is characterized through the turbulent kinetic energy ($k = \frac{1}{2}\langle u_i' u_i' \rangle$) and its rate of dissipation ($\varepsilon = \nu \langle u_{i,k}' u_{i,k}' \rangle$), the generalized relation which determines the turbulent viscosity ν_t takes the form[2]

$$\langle \nu_t \rangle = C_\mu f_\mu k^2/\varepsilon \tag{5}$$

The distributions of k and ε are determined through a straightforward application of flow decomposition (2) to the well-known model-transport equations for k and ε in steady-state (see [14]). The model coefficients are those of the standard k–ε model. These equations are solved together with those governing the mean flow. Note that the present approach gives rise to the definition of the time-averaged total kinetic energy,

$$k_{\text{tot}} = \frac{1}{2}\overline{\langle u_k' u_k' \rangle} = \frac{1}{2}\left(\overline{u_k' u_k'} + \overline{\tilde{u}_k \tilde{u}_k}\right) \tag{6}$$

which combines the mean turbulent kinetic energy $k = \frac{1}{2}\overline{u_k' u_k'}$ and the wave-induced or coherent kinetic energy, $k_{\text{coh}} = \frac{1}{2}\overline{\tilde{u}_k \tilde{u}_k}$.

[2] formulated here in the context of phase-averaging, i.e. with the symbol $\langle\ \rangle$.

4.1. Stress–strain relations

The algebraic representation of the Reynolds stress on the basis of second-order closure practice was first introduced by Rodi [15]. A variety of explicit algebraic stress models, with various levels of sophistication, followed, with the general aim of overcoming some of the defects of the Boussinesq linear representation of $\langle u_i' u_j' \rangle$. It is worth recalling that recourse to this modelling alternative was primarily motivated by what it retains of the major physical elements from second-order closures, but also by what it keeps from the simple architecture of the linear isotropic representation. Theoretically, the platform of these models is constructed on the basis of homogeneous turbulent flows in the limit of equilibrium [16]. In spite of this idealization, the strategy retains a factor of major physical relevance, namely the distinction between the components of the Reynolds stress tensor, though not accounting for their transport histories. Although a rigorous analysis of these models is beyond the scope of the present work, they can be roughly classified into many groups according to the formulation adopted for the eddy viscosity (isotropic or anisotropic), and to the model coefficients (constants, or based on one of the strain or vorticity invariants).

The extension of the Reynolds stress to non-linear form by invoking the Cayley–Hamilton series-expansion analysis was initially introduced by Pope [17]. A truncation of the generalized formulation of b_{ij}, the anisotropy tensor, to five linearly independent tensors ($(T_{ij})_n; n = 0, 4$), products of the strain and vorticity-rate tensors S_{ij} and Ω_{ij}, yields the following coordinate invariant form:

$$b_{ij} = \frac{\langle u_i' u_j' \rangle}{k} - \frac{2}{3}\delta_{ij} = -\frac{\langle \nu_t \rangle}{k} S_{ij} + \frac{\langle \nu_t \rangle}{\varepsilon}\left[\sum_{n=1}^{3} C_n \left(T_{ij}\right)_n + \frac{k}{\varepsilon} C_4 \left(T_{ij}\right)_4\right] \tag{7}$$

with

$$\left(T_{ij}\right)_1 = \left(S_{ik}S_{kj} - \frac{1}{3}S_{lk}S_{kl}\delta_{ij}\right)$$

$$\left(T_{ij}\right)_2 = \left(\Omega_{ik}S_{kj} + \Omega_{jk}S_{ki}\right)$$

$$\left(T_{ij}\right)_3 = \left(\Omega_{ik}\Omega_{kj} - \frac{1}{3}\Omega_{lk}\Omega_{kl}\delta_{ij}\right)$$

$$\left(T_{ij}\right)_4 = \left(S_{ki}\Omega_{lj} + S_{kj}\Omega_{li} - \frac{2}{3}S_{km}\Omega_{lm}\delta_{ij}\right)S_{kl} \tag{8}$$

and

$$S_{ij} = \langle u_{i,\,j} \rangle + \langle u_{j,\,i} \rangle; \qquad \Omega_{ij} = \langle u_{i,\,j} \rangle - \langle u_{j,\,i} \rangle \tag{9}$$

The model coefficients C_n (with $n = 1, 4$) for each of the employed models (to be introduced later) are given in Table 1. We recall that b_{ij} was formerly expressed in terms of 10 tensors $(T_{ij})_n$, with $(n = 0, 9)$, which are actually not all linearly independent. A novel trend to the traditional EASMs appeared with the work of Suga [18], followed by Craft et al. [19] and Lien et al. [20], who added the following third-order "cubic" tensors,

$$\frac{k}{\varepsilon}\sum_{n=6}^{7} C_n \left(T_{ij}\right)_n \tag{10}$$

where

$$\left(T_{ij}\right)_6 = \left(S_{ij}S_{kl}S_{kl}\right); \qquad \left(T_{ij}\right)_7 = -\left(S_{ij}\Omega_{kl}\Omega_{kl}\right) \tag{11}$$

with the view to cope with the effects of streamline curvature. It is evident that these additional terms can be gathered into the isotropic part of b_{ij}, so as to re-evaluate the coefficient C_0 (traditionally = 1); i.e. $C_0 = 1 - C_6(S^2 - \Omega^2)$, since $C_6 = C_7$ (see Table 1).

4.2. The modified algebraic stress models

The mathematical rationale which underpins the development of Gatski and Speziale's [16] (GS) fully-explicit algebraic stress model refers to integrity basis analysis. The expressions for the Reynolds stress, which enter the first two terms ($n = 1, 2$) of Eq. (7) are derived from the exact solution to the Reynolds stress transport equation, evoking the hypothesis of homogeneous turbulence in the limit of equilibrium. In short, the model can be viewed as an anisotropic eddy viscosity with unknown coefficients which depend on the constants of the pressure–strain correlation model (here, in particular, with reference to Speziale, Sarkar and Gatski [21] SSG, whose coefficients are reported in Table 1: α_n, $n = 1, 4$), and the invariants η^2 and ξ^2 (see Table 1).

Table 1
Constitutive relations and model coefficients of Eq. (7)[a]

Model	C_μ	C_1	C_2	C_3	C_4	C_6, C_7
SZL [31]	$\frac{1}{A_0+A_s\sqrt{S^2+\Omega^2}}$	0.0	$\frac{\sqrt{1-9C_\mu^2 S^2}}{2C_\mu(1+6S\Omega)}$	0.0	0.0	0.0
GS [16]	$\frac{\phi}{3-2\eta^2+6\xi^2}$	$\frac{2-\alpha_3}{2g}$	$\frac{1-\alpha_4/2}{2g}$	0.0	0.0	0.0
CLS [19]	$\frac{0.3f_3}{1+0.35\tilde{U}^{3/2}}$	−0.1	0.1	0.26	$-5C_\mu^2$	$-5C_\mu^2$
LCL [20]	$\frac{0.667}{1.25+S+0.9\Omega}$	$\frac{0.75}{1000+S^3}$	$\frac{3.75}{1000+S^3}$	$\frac{4.75}{1000+S^3}$	$-10C_\mu^2$	$-2C_\mu^2$

[a] $g = \alpha_1 + \frac{P}{\varepsilon} - 1$; $\alpha_1 = 3.4$; $\alpha_2 = 0.36$; $\alpha_3 = \frac{5}{4}$; $\alpha_4 = 0.4$; $\eta^2 = \frac{(C_1 S)^2}{4}$; $\xi^2 = \frac{(C_2\Omega)^2}{4}$; $\phi = \frac{4-3\alpha_2}{2g}$; $\tilde{U} = \mathrm{Max}(S, \Omega)$; $A_0 = 4.6$; $S = \frac{k}{\varepsilon}\sqrt{1/2 S_{lk}S_{kl}}$; $\Omega = \frac{k}{\varepsilon}\sqrt{1/2\Omega_{kl}\Omega_{kl}}$; $f_3 = 1 - \exp[\frac{-0.36}{\exp(-0.75\tilde{U})}]$; $A_s = \sqrt{6}\cos[\frac{1}{3}\arccos(\sqrt{6}W)]$; $W = \frac{S_{ij}S_{jk}S_{ki}}{(S_{ij}S_{ij})^{3/2}}$.

The constraint of "weak equilibrium" is, however, significant in that the model is not of practical utility away from the equilibrium limit. Yet, since conventional two-equation models are nothing more than particular cases of the non-linear expression for the Reynolds stress, this assumption would, in principle, compromise their application to complex turbulent flows. Nonetheless, Gatski and Speziale [16] reinforced this constraint by treating the production-to-dissipation ratio (P_k/ε), where

$$P_k = -\langle u_i' u_j' \rangle \langle u_{i,\,j} \rangle = -k b_{ij} S_{ij}, \tag{12}$$

encompassed in the expressions for C_1 and C_2 in Table 1, through the equilibrium solution for homogeneous turbulence. This solution, which has been initially adopted for the SSG pressure–strain model [21], omits to represent the transport effects in the k- and ε-equations, and yields the equilibrium value $P_k/\varepsilon = (C_{\varepsilon 2} - 1)/(C_{\varepsilon 1} - 1) \approx 1.89$ (i.e. $g = 0.233$ in Table 1). In effect, such an alternative helps alleviate the singularities of the effective viscosity which can arise when P_k/ε is treated implicitly [22]. Later, however, the necessity to account for the changes in the production-to-dissipation-rate ratio P_k/ε was fully acknowledged [23,24], because, its equilibrium value drives the model to inconsistency when used away from equilibrium.

As a remedy, Grimaji [23] has developed a fully-explicit, self-consistent variant of the GS model, by solving the cubic equation for P_k/ε arising in the context of the selected pressure–strain model [23]. The resulting solution for P_k/ε is unfortunately too cumbersome to be easily implemented in existing codes. However, this achievement yielded a new model variant which, in the case of irrotational straining, i.e. $\xi \approx 0$, departs significantly from the regularized model in that C_μ decreases with increasing η. Recently, Jongen and Gatski [24] have extended the same GS model through a new approach for characterizing the equilibrium states of the Reynolds stress anisotropy in homogeneous turbulence. Their model consists of a generalized relationship for P_k/ε which can cover all planar homogeneous flows, with and without rotation.

Here, we aim at extending the forgoing effort to make the GS model applicable to a broad range of practical flows. To that end, we emphasize on the following two points, though always in the context of a mild departure from equilibrium: (i) the development of a generalized relation for P_k/ε, which can reasonably mimic both Grimaji's [23] and Jongen and Gatski's [24] models, and (ii) the formulation of a more accurate regularization procedure. The new calibrated relation for P_k/ε will serve to determine the coefficients C_1 and C_2, while it must recover, at least, the established equilibrium values for both the logarithmic region in a turbulent boundary layer, and the homogeneous shear flow. Based on the characteristics of both type of flows, and owing to the property $\lim_{S\to\infty} P_k/\varepsilon \sim S$ [24], the following formulation for the production-to-dissipation ratio is proposed:

$$\frac{P_k}{\varepsilon} = \frac{S^2}{4.8 + 1.3\max(S, \Omega)} \tag{13}$$

where S and Ω are given in Table 1. It can be easily seen that the proposed relation meets the requirement of the equilibrium state $P_k/\varepsilon \approx 1$ for the logarithmic region in channel flow, where,

by reference to Laufer's [25] data, $S = 3.1$. The calibration of Eq. (13) for homogeneous shear flow follows, however, the scale expansion theory for the Reynolds stress by reference to Speziale and Mac Giolla Mhuiris [26]. The starting point consists in using the "conventional" isotropic closure for the deviatoric part of the Reynolds stress in Eq. (7), i.e. $\langle \tau_{ij} \rangle = -C_\mu (k^2/\varepsilon) S_{ij}$. The dimensionless variable $k^+ = k/k_0$ is then introduced, where k_0 refers to the initial turbulent kinetic energy. In so far as the case of homogeneous shear flow nullifies $\nabla^2 k$ and $\nabla^2 \varepsilon$ in their transport equations, the deviatoric part of Eq. (7) and the dissipation equation take the following simple forms:

$$\frac{\mathrm{d}k^+}{\mathrm{d}t^+} = k^+ \left(C_\mu S - 1/S \right),$$

$$\frac{\mathrm{d}S}{\mathrm{d}t^+} = -C_\mu (C_{\varepsilon 1} - 1) S^2 + (C_{\varepsilon 2} - 1), \tag{14}$$

where $t^+ = S \cdot t$. Setting now $\mathrm{d}S/\mathrm{d}t = 0$, we obtain the single point of the above equation

$$S_0 = \left[(C_{\varepsilon 2} - 1)/C_\mu (C_{\varepsilon 1} - 1) \right]^{1/2}, \tag{15}$$

which, in the context of the GS model ($C_{\varepsilon 1} = 1.44$, $C_{\varepsilon 2} = 1.83$, and the equilibrium value of $C_\mu \approx 0.094$ for shear flow is invoked) converges towards $S_0 = 4.48$. This single value permits the equilibrium state to be correctly recovered through $P_k/\varepsilon(S_0) = 1.89$. In Fig. 1, relation (13)

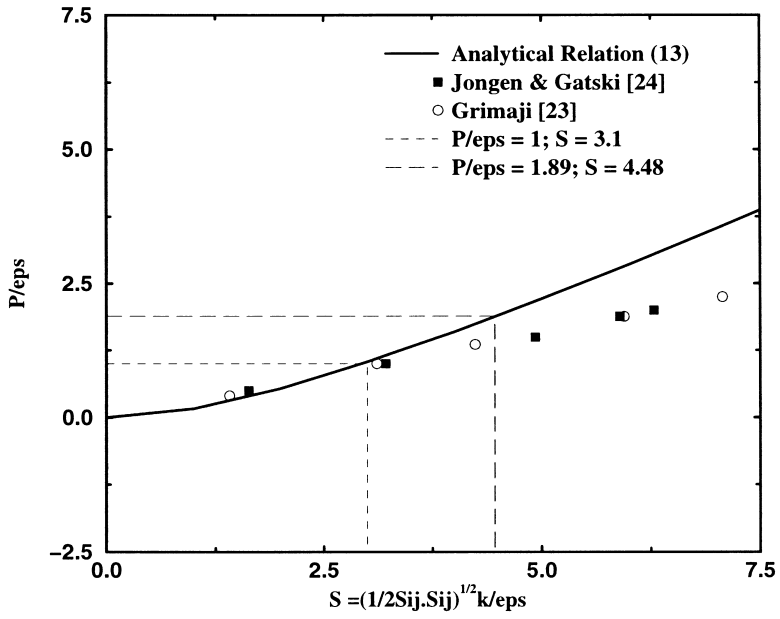

Fig. 1. Locus of solution points for P_k/ε as a function of $S = \Omega$.

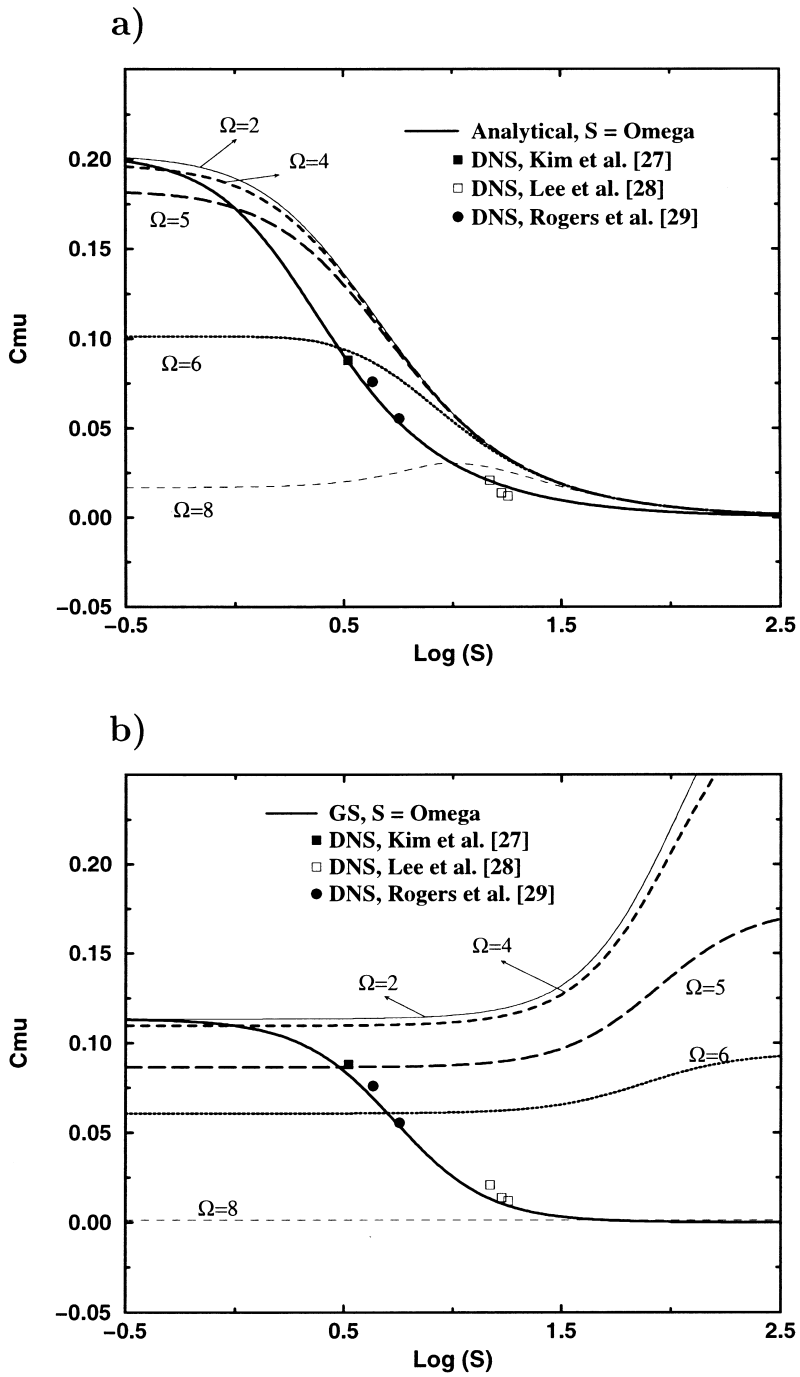

Fig. 2. Distribution of C_μ as a function of S and Ω: (a) with the modified GS model; (b) with the GS model.

is illustrated and clearly shown to recover the self-consistent models of Grimaji [23] and Jongen and Gatski [24] for weak departures from equilibrium ($S < 5$). While it is a simple matter to show that making use of Eq. (13) does not affect the exponential growth of $k^+ \propto e^{\lambda t^+}$ (λ refers to the rate of growth [26]), this relationship returns, however, a C_μ distribution (Fig. 2a) that deviates significantly from that displayed in Fig. 2b — results are compared with various DNS data, i.e. [27–29]. As shown in Fig. 2a, the result is, in fact, very similar to that of the self-consistent model of Grimaji [23]. It should be noted that the result shown in the latter figure confirms the note of warning constantly evoked by Speziale [22] with regard to the repercussions that might follow from fixing P_k/ε. As a flagrant example, the GS model is unlikely to predict an impinging flow because C_μ has the potential to grow and thereby to drastically overestimate the eddy viscosity in Eq. (7). This can lead to the prediction of non-physical (negative) normal stress components, and thereby violate the realizability principle.

It is anyway recognized [22] that, in highly-strained flows, $\eta \gg 1$, which nullifies the validity of the regularization procedure developed by Gatski and Speziale [16], resorting to a first-order Padé approximation for η^2; i.e. $\eta^2 \approx \eta^2/1+\eta^2$. This latter practice was simply abandoned in the present work for a more elaborate formulation which invokes an approximation that is accurate to the fourth order of η, though different from those reported recently by Speziale [22]. It takes the following form:

$$\eta^4 \approx \frac{\eta^4}{1+\eta^4}; \quad \text{or} \quad \eta^2 \approx \frac{\eta^2}{\left(1+\eta^4\right)^{1/2}} \tag{16}$$

and gives rise to

$$C_\mu = \frac{\phi\left(1+\eta^4\right)}{3+\eta^4\left(1+6\xi^2\right)-2\eta^2+6\xi^2} \tag{17}$$

This systematic regularization represents so far an excellent approximation to the original $C_\mu = \phi/(3-2\eta^2+6\xi^2)$ for turbulent flows near equilibrium (η and $\xi < 1$), and a much better alternative to the first-order one for flows that are near equilibrium. Moreover, the expression in Eq. (14) is regular for all values of η and ξ, and has the correct asymptotic behaviour of $C_\mu/\phi \approx 1/\eta^2$ for $\eta \gg 1$.

Finally, to close this description, the extension of the corrected model to low-*Re* conditions is achieved here by invoking a similar model-function f_μ to that of the one-equation model of Norris and Reynolds [30], and adopts Jones and Launder's [14] damping of the destruction of dissipation.

The constitutive relation applied to yield the algebraic Reynolds stress model of Shih, Zhu and Lumley [31] (SZL) was obtained using the invariance theory in continuum mechanics, while invoking the constraints based on rapid distortion theory and turbulence realizability. The model was deliberately truncated by the authors to its tensorial quadratic form. In the present situation, however, the model was used in its linear form ($C_n = 0, n > 1$) as an alternative (rather than employing ad-hoc methods), to reduce the excessive rate of turbulence production P_k that can be generated by conventional models at flow impingement through $P_k = C_\mu \varepsilon S^2$. In this type of closure, the normal stresses determined through $\langle u_i' u_i' \rangle = 2k/3 -$

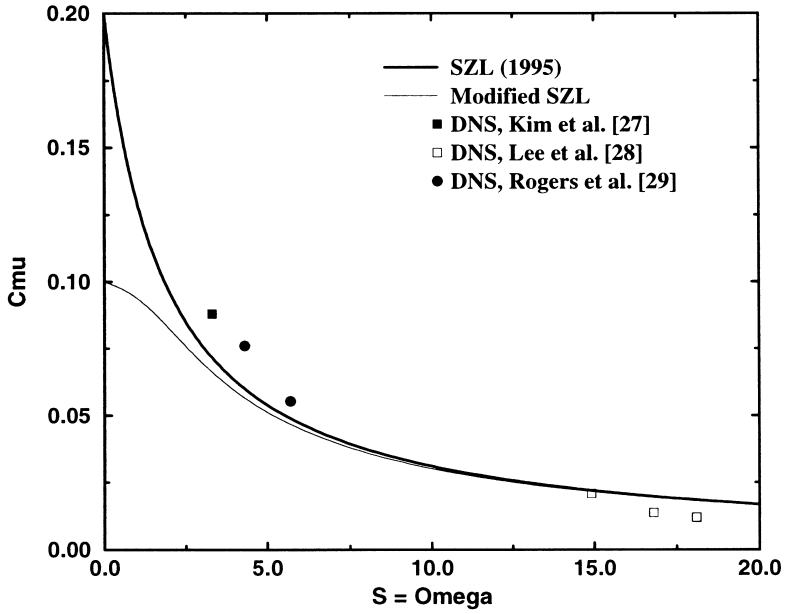

Fig. 3. Distribution of C_μ as a function of $S+\Omega$, obtained with the modified SZL model.

$C_\mu k^2/\varepsilon S_{ii}$ are not distinct, and may become negative for large positive strain rate S_{ii}, which then violates the realizability principle. It clearly arises that, in absence of high-order, non-linear stress–strain products forming b_{ij}, physical consistency requires special treatments for alleviating such a shortcoming, namely by imposing a constraint exclusively on C_μ. Now, because the original model was found to return very high C_μ values for simple homogeneous flows, the following correction was adopted as a remedy.[3]

$$C_\mu = \frac{1}{A_0 + A_s\sqrt{S^2+\Omega^2}}; \qquad \text{with } A_0 = 10.2 - 5.5\tanh(0.55S) \tag{18}$$

which differs from its original version in the way the coefficient A_0 is modelled, rather than being assigned a value falling within the interval $4.0 < A_0 < 6.5$ [31]. The coefficient A_s is defined in Table 1. As is to be expected, the behaviour of the modified expression for C_μ, illustrated in Fig. 3, departs significantly from the one proposed originally.

The Low-*Re* model of Abe et al. [32] (hereinafter referred to as AKN), which introduces the Kolmogorov velocity scale $u_\varepsilon = (\nu\varepsilon)^{1/4}$ instead of the velocity scale $k^{1/2}$, is employed for the near-wall direct integration. The closure constants are assigned the non-standard values proposed by them, i.e $C_1 = 1.5, C_2 = 1.9$, and $\sigma_k = \sigma_\varepsilon = 1.4$. The boundary conditions employed for this model consist of the no-slip condition on the wall surface, k is set equal to zero, while the strict boundary condition for ε, i.e. $\varepsilon_w = 2\nu(\partial^2/\partial n^2)$, is approximated using the

[3] This could also have been achieved by specifying an upper bound for C_μ.

relation $\varepsilon|_{\text{wall}} = 2\nu k/y_n^2$. To avoid numerical instabilities, this treatment has been applied at the first grid-nodes neighbouring the wall, rather than on the wall itself. The combination of these two approaches which consists in replacing $C_\mu = 0.09$ in the AKN model by Eq. (18) is hereafter referred to as SZL + AKN.

4.3. The selected algebraic stress models

The EASM of Lien, Chen and Leschziner [20] (LCL) adopts the Shih et al. [31] concept, which consists in sensitizing both the eddy-viscosity and the coefficients C_n to the strain invariant S defined in Table 1. In addition, the revised model claims to cope with effects of streamline curvature by including the cubic terms proposed by Suga [18]. The eddy viscosity is damped using a similar function to the Norris and Reynolds' [30] one-equation model, while $f_{\varepsilon 2}$ is introduced with reference to the Jones and Launder [14] prescription. The closure constants are assigned the standards values [14].

In the EASM of Craft, Launder and Suga [19] (CLS), the constitutive relations linking the stresses to the velocity gradients integrate the cubic terms with reference to Suga's [18] model as well. Originally, the model was proposed to remedy the spurious normal strain-induced production of turbulence resulting from the conventional isotropic concept. The approach follows the Jones and Launder [14] model in regard to the model functions of the ε-equation.

4.4. The proposed zonal Reynolds stress model

It is now recognized that the difficulties encountered in employing second-order closures are due to their cumbersome structure rather than to the computational costs involved in solving the additional differential equations for individual turbulent stresses. It is also argued that their direct integration to solid walls using no-slip conditions for velocity is, to date, not viable and constitutes an additional numerical complexity. This might partially explain, to the best knowledge of the authors, that there exists no single, successful attempt reported for computing vortex-shedding flows with the aid of a pure RSM in low-*Re* conditions since the work of Franke and Rodi [6]. Although the results of combining the Launder, Reece and Rodi [33] model (LRR) with a linear, near-wall, one-equation model by these authors were better than most of the previous attempts, there still exists an uncertainty with regard to the coupling of the explicitly-computed Reynolds stress components to the modelled ones. One approach to help alleviate such difficulties is proposed here and consists in linking dynamically (without fixed grid-layers) an outer RSM to a near-wall, one-equation, non-linear model in which the turbulence stresses are determined from stress–strain relationships (Eq. (7)). This ensures smooth matching between the zones and, ideally, the strong near-wall anisotropy of the stresses can then be captured.

In the one-equation turbulence model to be employed in the near-wall region, the eddy viscosity is made proportional to a velocity scale ($k^{1/2}$) and a length scale (l_μ). The distribution of (l_μ) is prescribed algebraically, while the velocity scale is determined by solving the transport equation for (k), together with the mean flow equations. The dissipation rate (ε) appearing as a sink term in the k-equation is related to k itself, and a dissipation length scale l_ε which is also

prescribed algebraically. It should be mentioned that in the viscous sublayer l_μ and l_ε deviate from the linear dependence on distance from the wall in order to account both for the damping of ν_t and the limiting behaviour of ε at the wall. The one-equation turbulence model employed here is due to Wolfshtein [34] and reads:

$$\nu_t = C_\mu k^{1/2} l_\mu; \quad l_\mu = C_l\, y_n \underbrace{\left[1 - \exp\left(-R_y/A_\mu\right)\right]}_{f_\mu} \tag{19}$$

$$\varepsilon = k^{3/2}/l_\varepsilon; \quad l_\varepsilon = C_l y_n \left[1 - \exp\left(-R_y/A_\varepsilon\right)\right] \tag{20}$$

The exponential reduction (f_μ between brackets) of the length scale l_μ involves the near-wall Reynolds number $R_y = k^{1/2} y_n/\nu$. The constant C_l is set equal to $\kappa C_\mu^{-3/4}$ to conform to the logarithmic law of the wall (κ is the von Kármán constant), while $A_\varepsilon = 2C_l$ is set in order to reproduce the asymptotic behaviour of $\varepsilon|_{\text{wall}} = 2\nu k/y_n^2$. The empirical constant appearing in the damping function f_μ is assigned the standard value $A_\mu = 70$ [34].

The phase-averaged, Reynolds-stress transport equations can be expressed in the following compact form

$$\frac{\partial \langle \tau_{ij} \rangle}{\partial t} + \frac{\partial \langle u_k \rangle \langle \tau_{ij} \rangle}{\partial x_k} = \langle D_{ij}^{\mu} \rangle + \langle D_{ij}^{T} \rangle + \langle P_{ij} \rangle + \langle \Phi_{ij} \rangle - \langle \varepsilon_{ij} \rangle \tag{21}$$

where production and molecular diffusion are designated by the terms $\langle P_{ij} \rangle$ and $\langle D_{ij}^{\mu} \rangle$, respectively. Both the pressure–strain correlation $\langle \Phi_{ij} \rangle$ and turbulent diffusion $\langle D_{ij}^{T} \rangle$ need to be modelled. In the present case, $\langle D_{ij}^{T} \rangle$ is modelled using the generalized gradient diffusion approach of Daly and Harlow [35], and incorporates the damping function f_μ appearing in Eq. (19):

$$\langle D_{ij}^{T} \rangle = \frac{\partial}{\partial x_k} \left[\left(\rho C_s f_\mu \langle \tau_{kl} \rangle \right) \frac{\partial \langle \tau_{ij} \rangle}{\partial x_l} \right] \tag{22}$$

Modelling of $\langle \Phi_{ij} \rangle$ follows Gibson and Launder's [36] proposal for the wall reflection terms and employs the coefficients of the IP pressure–strain model proposed by Gibson and Younis [37] (GY), i.e. $\alpha_1 = 3.0$, $\alpha_2 = 0.8$, $\alpha_3 = 1.2$, $\alpha_4 = 1.2$, and $g = 4.0$. The transport equations for the Reynolds stress tensor are solved together with a transport equation solving the turbulence energy dissipation rate ε. Within the viscous sublayer, the Reynolds stresses appearing in the momentum equations are determined through stress–strain relations, retaining, as in [16], terms up to the quadratic products of the strain and vorticity tensors in Eq. (7), i.e. $C_n(T_{ij})_n = 0$ for $n = 3, 7$. The model coefficients C_1 and C_2 are determined following Gatski and Speziale's [16] paths in the derivation of their SSG-based EASM; they read $C_1 = 0.1$, $C_2 = 0.05$ and $\phi = 0.2$ (see Table 2 for $C_n = f(\alpha_n)$). It should be noted, however, that C_μ is assigned here its standard value 0.09 in order to match the constant $C_l = \kappa C_\mu^{-3/4}$ at the edge of the viscosity-affected layer.

It is relevant to note that various other well known pressure–strain models were tested, but without success, including that of Speziale, Sarkar and Gatski [21]. The outer RSM and the

non-linear, near-wall model are matched dynamically at a location where viscous effects become negligible, i.e. where the near-wall Reynolds number $R_y = k^{1/2} y_n/\nu = 80$; this choice is made on the basis of DNS data from channel and boundary layer simulations, as explained by Lakehal and Rodi [38]. The proposed dynamic zonal strategy differs from classical two-layer approaches in which two sub-domains are distinct. Here, both the one-equation model and the RSM are solved separately, everywhere in the domain, then both solutions are compared: in flow regions where $R_y < 80$, the RSM solutions are clipped and replaced by those obtained by the one-equation model.

5. Computational methodology

5.1. Numerical procedure

The two-dimensional version of the Navier–Stokes equations solver ELAN was employed for the computations. The algorithm consists of a semi-structured, multi-block, multi-grid finite-volume method. The structure of the code is based on the strong conservation form within general, body-fitted coordinates, and employs a fully co-located storage arrangement for all quantities. In this, diffusion terms are approximated using second-order central differences, whereas advective fluxes can be approximated using various high-order bounded (monotonic) schemes, the latter applied in scalar form by means of a deferred-correction procedure. The present computations were performed employing the well known QUICK scheme to all variables, the truncation error of which is proportional to the third power of grid size and fourth-order derivative of velocity. The odd–even decoupling problem of the cell-centred scheme is suppressed with a fourth-order, artificial-dissipation apparent pressure term in the continuity equation. The solution is iterated to convergence using a compressible (all-speed) pressure-correction approach. The temporal discretization consists of a second-order, back-step scheme for all variables.

5.2. Grids and boundary conditions

The dimensions of the computational domain were set as follows: each lateral boundary is located at $6D$ from the centre line, the inflow and outflow planes being $4.5D$ upstream and $15D$ downstream the cylinder, respectively. Grid-independent results were obtained with a refined mesh consisting of 226×156 grid points[4] in the x- and y-directions. The computation domain and grid are shown in Fig. 4. Solving Accurate solution of the system was found to be closely related to the grid concentration in near-wall regions, in particular, for the models in which the stress–strain model coefficients C_n depend on the irrotational strain η^2 (or S^2), the near-wall gradient of which is very steep. The additional grid-sensitivity which was made on the finest

[4] All the references cited in here, i.e. [5–8], have employed a coarser grid than the present one.

grid in order to clarify the importance of near-wall grid concentration, has shown that the first control volume neighbouring the wall must be placed at a location where $y^+ < 1$.

At the inflow plane, a constant streamwise velocity was prescribed, while k and ε-profiles were specified using uniform distributions corresponding to a free-stream turbulence intensity of $T_u = 2\%$, and a rate of dissipation based on length-scale $L_u/D = 0.8$, i.e. $(\varepsilon = C_\mu^{3/4} k^{3/2}/\kappa L_u)$. It is important to note that none of the experiments has reported

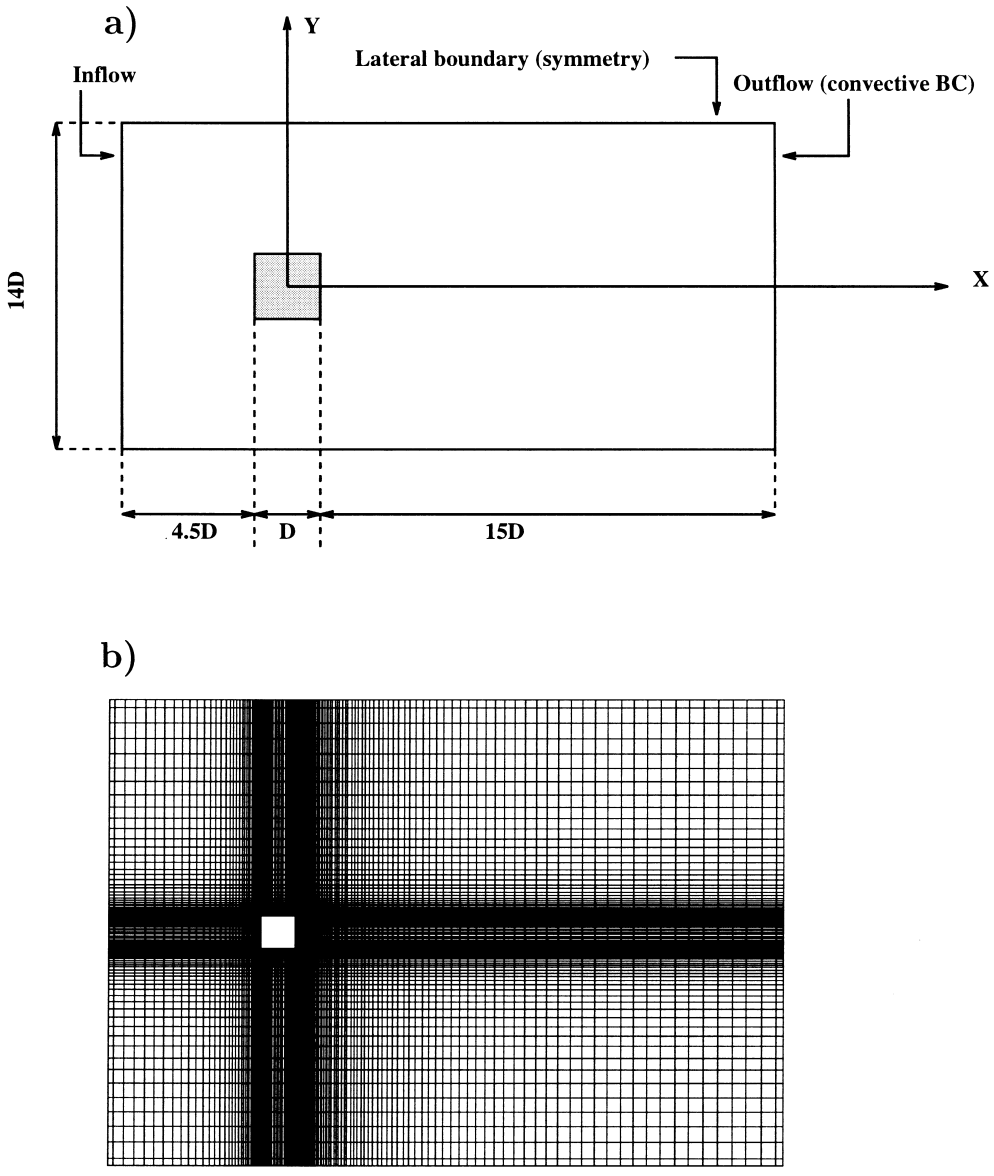

Fig. 4. Flow configuration (a) and computational grid (b).

information concerning the length-scale for this rate of turbulence intensity. The choice of such a level of L_u/D may be questionable if one considers the laminar-turbulent transitional nature (which is reported in Lyn's et al. [3] experiment) of the flow (L_u is probably much smaller). However, in a recent work investigating the implications of inflow conditions of turbulence (to be submitted), the authors have found that similar results can be obtained with a linear and non-linear low-*Re* model (e.g. SZL), for different levels of imposed length-scale, i.e. $L_u/D = 0.1$ and 0.8. The other reason for our choice of L_u/D is to permit a coherent comparison with the previous investigations, and in particular, with Franke and Rodi's [6] RSM results. Non-reflective conditions were employed at the outflow cross-section for velocity components and individual Reynolds stresses (RSM), whereas a condition of zero-gradient was imposed for all other variables. In total, 40 h CPU time on the Cray T90 vector machine at the University of Kiel, Germany, were needed to perform 30 periods; each necessitating approximately 400 time-steps of $\Delta t = 0.02S$, depending on the predicted Strouhal number. The system of equations was iterated till the mass–flux residuals were reduced by three orders during each time step. We also note that the number of inner iterations per time step was about two orders of magnitude higher than for the RSM computations.

6. Discussion of results

6.1. Effects of the numerics and inflow conditions

The sensitivity of numerical schemes, grid dependence, time step variations, boundary conditions, etc., were studied in two separate works (see [1,2]). Noteworthy is to recall the major findings, some of which are actually well known, such as the absolute requirement for a high-order discretization scheme. It was found that a minimized expansion ratio between the cross-stream grid-lines ($\Delta x_i/\Delta x_{i-1} < 1.1$) is required for structured grids, because otherwise any high-order discretization scheme would lose accuracy. However, adopting non-reflective boundary conditions rather than conventional zero-gradient ones did allow to significantly reduce the dimensions of the computational domain, in comparison with previous contributions in which the outer boundary was extended up to $60D$ [8]. Employing these non-reflective conditions was also relevant for predicting the time to the first vortex-shedding.

With regard to inflow conditions of turbulence, the computations employing any of the low-*Re* isotropic models on the basis of a length-scale $L_u/D > 0.5$ (i.e. $\nu_t \approx 50 \times \nu$) did not succeed. This may partially explain the relative success of Bosch [5] with the standard k–ε model, who opted for $\nu_t = 10 \times \nu$, in comparison with Franke and Rodi [6] who used $\nu_t = 100 \times \nu$. This observation is valid for low-*Re* model calculations as well: for instance, Kawamura and Kawashima [7] have had success with $\nu_t \approx 20 \times \nu$. Many other authors, such as Deng et al. [8], report however that they failed to calculate this flow with a pure low-*Re* model, and it is not impossible that it was simply due to their choice[5] of L_u/D. This finding has motivated an

[5] Deng et al. [8] did not report information concerning the imposed length-scale L_u/D.

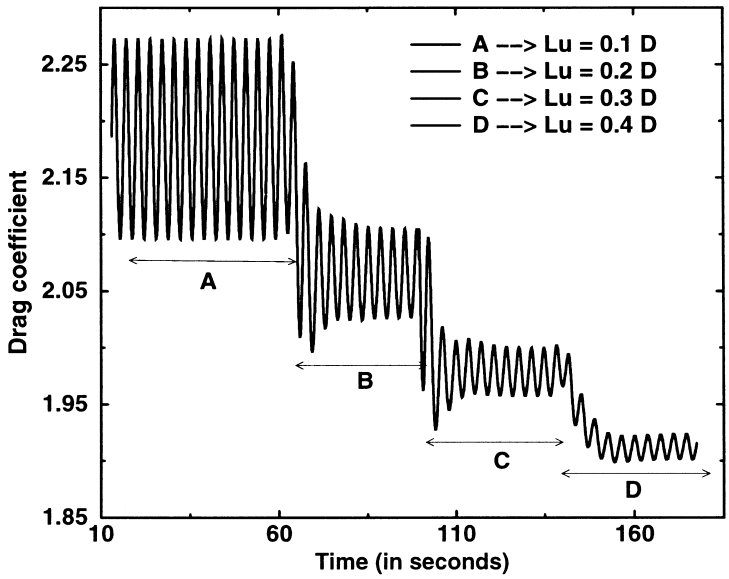

Fig. 5. Time evolution of the drag signal with increasing inflow length-scale. Computations with the AKN low-*Re* model.

analysis of the implications of freestream turbulence in modelling this flow (results to be submitted), the main results of which are discussed in the context of Fig. 5. The figure reports the temporal evolution of the mean drag coefficient obtained with the linear, low-*Re* model (AKN), with varying imposed turbulent length-scale L_u/D. It is clear that, in all cases, the model predicts the shedding motion and indicates that a vortex-shedding flow may be adequately described by a simple linear model which solves the viscosity-affected layer, provided the method of solution is rigorously accurate, and realistic inflow conditions of turbulence are imposed. According to the figure, there is a strong dependence on the variation of L_u/D through a significant reduction in the drag amplitude. However, the dimensionless frequency of shedding *St* was found to be unaffected by changes in L_u/D. It appears that employing an EVM with a certain degree of imposed length-scale ($L_u/D \geq 0.5$) dampens the shedding dynamics, as a result of the addition of the spurious effective viscosity generated in the stagnation flow regions to the imposed one (through L_u/D).

In the following, attention is focused on the behaviour resulting from the use of the modified modelling closures (SZL and GS), along with the new zonal RSM approach (GS + TLW) proposed in this work. The comparison of both integral coefficients and time-averaged quantities includes, however, results of the CLS and LCL algebraic Reynolds stress models.

6.2. Global forces

Fig. 6 shows *typical* time intervals of the drag coefficients obtained with different modelling strategies. It indicates that all models predict fairly well the vortex shedding motion, in

Table 2
Global parameters from experiments, LES, EASM, and RSM calculations[a]

	Re	$\bar{C}_d$	$\tilde{C}_d$	$C_{d,\,rms}$	$\tilde{C}_l$	$C_{l,\,rms}$	St	l_r
Contribution								
Exp. [3]	2.2×10^4	2.10	–	–	–	–	0.132	1.38
Exp. [4]	1.4×10^4	2.0–2.2	–	–	–	–	0.139	–
Exp. [44]	17.6×10^4	2.05	–	0.23	–	1.22	0.122	–
Exp. [45]	$2–7 \times 10^4$	2.15	–	–	–	–	0.125	–
LES								
UTK [10], S1	2.2×10^4	2.10	0.12	0.20	1.58	–	0.132	–
ECL [2], S1	2.2×10^4	2.57	–	0.32	–	1.58	0.11	1.22
UKA2 [11], S2	2.2×10^4	2.30	–	0.14	–	1.15	0.13	1.46
TAMU2 [11], S2	2.2×10^4	2.77	–	0.19	–	1.79	0.14	0.94
EASM								
Present (SZL-AKN)	2.2×10^4	2.27	0.158	0.105	2.04	1.380	0.149	1.09
Present (GS-modif.)	2.2×10^4	2.28	0.165	0.108	2.08	1.359	0.150	1.23
Present (CLS)	2.2×10^4	2.77	0.135	0.107	2.12	1.534	0.135	1.22
Present (LCL)	2.2×10^4	2.18	0.128	0.187	2.08	1.538	0.128	1.22
RSM								
[6] (LRR-NR)	2.2×10^4	2.43	0.079	0.06	1.84	1.3	0.159	1.00
Present (GL-W)	2.2×10^4	2.24	0.105	0.067	1.77	1.07	0.153	1.28

[a] Two-Layer (NR: Norris and Reynolds; W: Wolfshteiin). S1: Smagorinski; S2: Dynamic SGS.

particular, the modified GS (the original regularized version failed; no shedding was predicted). The figure suggests that a clear Strouhal number can be determined from each result, and the amplitude of the main mode $\tilde{C}_d$ strongly depends on the nature of the model. Simply, the resulting drag signal is almost regular with calculations using the linear SZL model, while significant lower to higher frequency modulation of its amplitude appears with increasing order of the non-linear terms of b_{ij}. This finding contrasts somewhat the accepted argument [6] which states that, by imposing two-dimensionality to the mean flow, the RANS concept is supposed to yield a regular shedding motion. It is also interesting to note that the amplitude of the main mode $\tilde{C}_d$ delivered by the RSM model is the smallest, as confirmed in Table 2. The same trend can be seen on time evolutions of the lift coefficient C_l in Fig. 7; it clearly indicates a significant influence of non-linear expressions of Reynolds stress on the behaviour of each model, be they algebraically determined (GS and CLS) or individually calculated (GL + TLW). Again, results of the anisotropic, eddy-viscosity model SZL show regular modulation, while the strong lower to higher frequency variation is now truly established as being the result of transcending the conventional eddy-viscosity approach. In comparison with Murakami's [10] LES data, Table 2 indicates that nearly all algebraic stress models overpredict both $C_{d,\,rms}$ and $C_{l,\,rms}$, while a noticeable improvement is brought about by the RSM. Most notably, though not reported in Table 2, is that $\bar{C}_l$ delivered by the RSM was equal to $\bar{C}_l = -0.03$, revealing thereby the asymmetric shedding above and below the wake centerline, as was the case in most of the LES reported in [11].

The particular irregularity of the shedding dynamics obtained using the RSM is intriguing.

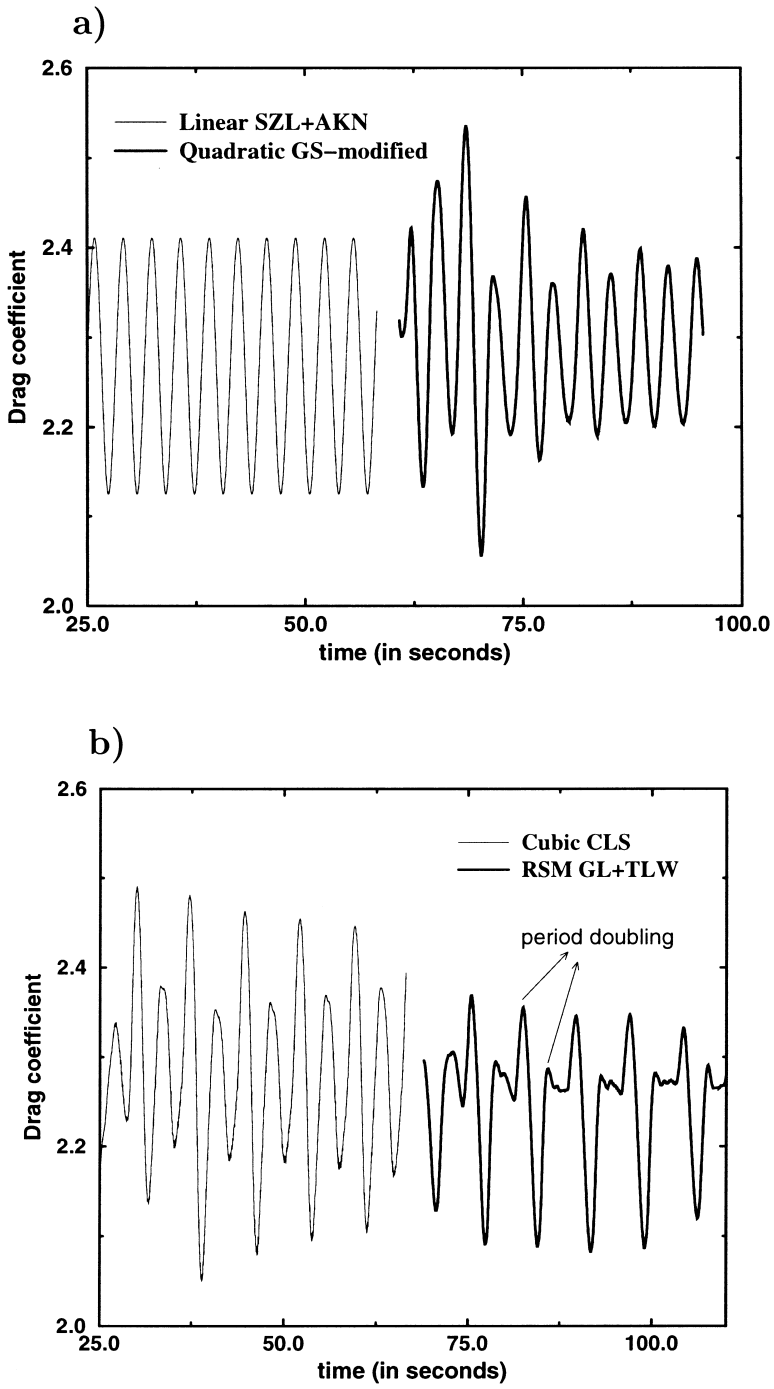

Fig. 6. Time intervals of the drag coefficient obtained with the different models: (a) linear and quadratic; (b) cubic and RSM.

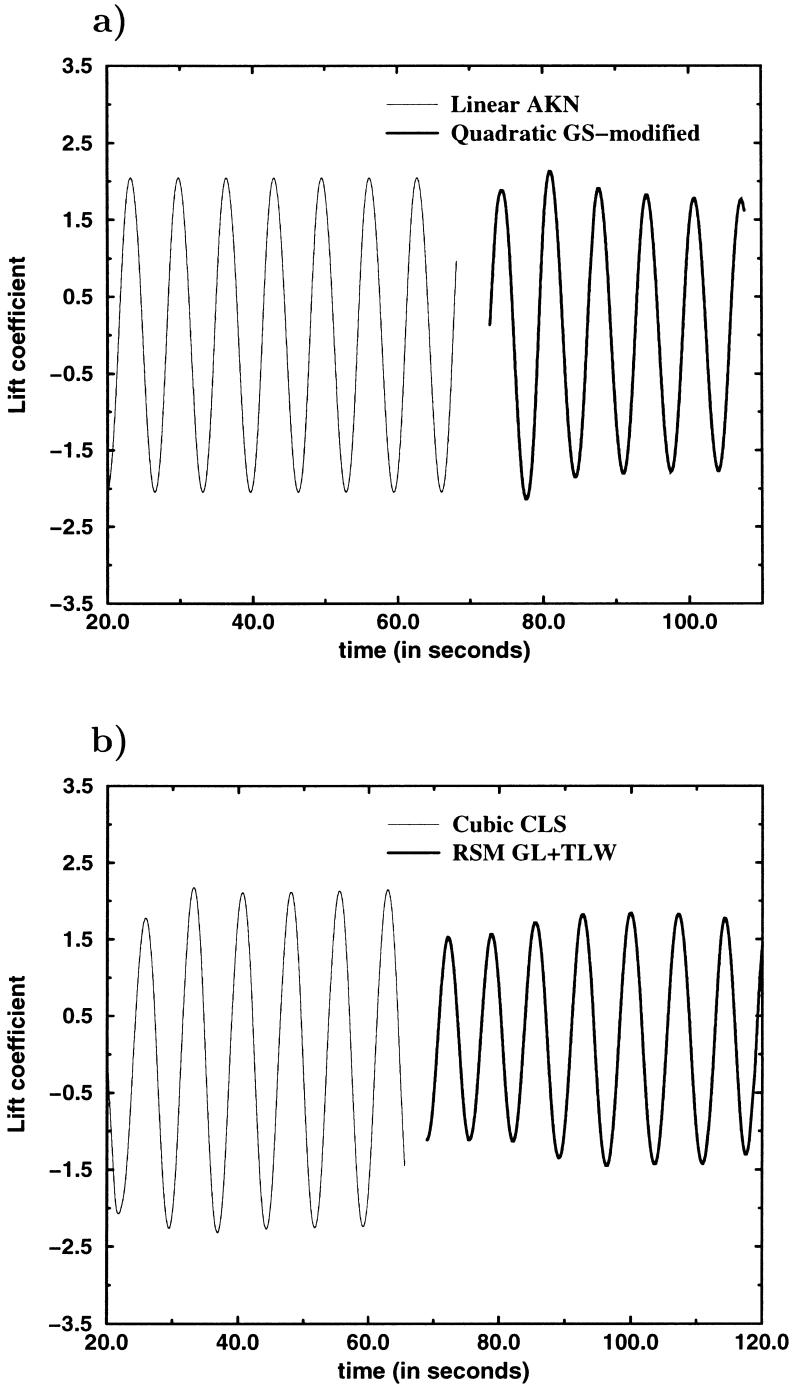

Fig. 7. Time intervals of the lift coefficient obtained with the different models: (a) linear and quadratic; (b) cubic and RSM.

The drag spectra, in particular, exhibits a phenomena known as the *period doubling*, extensively studied by Karniadakis and Triantafyllou [39]. The existence of the phenomenon was identified by them using DNS as being the signature of a fast transition from a laminar, two-dimensional régime to a turbulent state for the flow past a circular cylinder at $200 < Re < 500$. Similar results have been recently reported by Sohankar et al. [40] for flow past both a 2D square cylinder and a circular cylinder, again using DNS, and for a similar range of Reynolds numbers. It was, however, noticed that the phenomenon was not present in their 3D simulations. Robichaux et al. [41] have very recently performed DNS of the flow past the square cylinder, and have noticed the onset of mode A- and B-type three-dimensional disturbances, in line with what has been so far observed in studying the flow past the circular cylinder. Furthermore, they have detected the presence of a third intermediate wave-length mode, referred to as mode S instability, and which apparently results in an asymmetric shedding about the centerline. In his experimental analysis of similar shedding flows, Henderson [42] concluded that periodic doubling stems from forcing two-dimensionality on the flow by reducing the spanwise length of the cylinder. All the works cited share the same conclusion, however, that the wake undergoes transition to turbulence following the period-doubling process. In our case, though the Reynolds number is much higher, Lyn's experiment [3] has clearly shown that the flow is two-dimensional in the mean and is laminar upstream, and undergoes transition in the wake. Moreover, a laminar flow calculation of this flow at $Re = 2.2 \times 10^4$ by Deng et al. [8] yielded a secondary nondimensional frequency as well. These observations lend support to the prediction of periodic doubling by our zonal RSM model; a conclusion that remains tentative, however, due to lack of appropriate experimental data at $Re = 22{,}000$. They also contradict the forgoing speculation [39] which states that period doubling scenario leads to a chaotic wake at high Reynolds numbers. Beyond this mystery of period doubling at such high Reynolds number, when considered from a physical point of view, the results prove that the effective viscosity occuring in the entire flow-field must be rather low.

The resulting global forces obtained from different modelling approaches are compared with the experiments in Table 2. Entries include the dimensionless shedding frequency St, the time-averaged drag coefficient $\bar{C}_\mathrm{d}$, the phase-averaged drag and lift coefficients $\tilde{C}_\mathrm{d}$ and $\tilde{C}_\mathrm{l}$ (or amplitudes of the main mode), the RMS values of the temporal variation of drag and lift coefficients $C_{\mathrm{d,\,rms}}$ and $C_{\mathrm{l,\,rms}}$, and the length of the time-averaged separation in the wak l_r (estimated from the centre of the cylinder). In addition, the table includes various LES results,[6] those of Murakami's group, referred to as UTK, two others from selected contributors to the *LES Workshop* of Rodi et al. [11], namely UKA2 and TAMU2, and the more recent ones (ECL) reported in [2]. The RSM results of Franke and Rodi [6] are also included because they represent still a reference point in this area.

The Strouhal number St obtained from both the SZL and GS models is overpredicted, and the same is true of the mean drag coefficient $\bar{C}_\mathrm{d}$. The shorter reattachment length in the wake predicted by the anisotropic eddy-viscosity model SZL, along with the overestimated drag

[6] UTK: University of Tokyo; UKA2: University of Karlsruhe; TAMU2: Tokyo Institute of Technology; ECL: Ecole Centrale de Lyon.

coefficient, indicate an exaggerated rate of momentum exchange in this region. This is a possible result of over-suppression of turbulence production P_k in front of the cylinder due to the modified relation for C_μ. Furthermore, the predicted shedding frequency exhibits a noticeable reaction to turbulence modelling using stress–strain expressions, decreasing towards the measured level with increasing order of strain and vorticity products of b_{ij}. Nonetheless, the algebraic Reynolds stress models give satisfactory agreement between calculation and measurement for $\bar{C}_\mathrm{d}$, and, against all expectations, much better than the most recent LES results. Incorporation of the Suga's [18] triple strain–strain and strain–vorticity correlations, $n = 6$ and 7, in both models CLS and LCL seems to bring a significant improvement over the quadratic GS approach through the prediction of a better Strouhal number and drag coefficient. However, this picture of superiority does not extend to all other parameters, such as the length of separation in the wake l_r, which remains unchanged for both the EASMs,

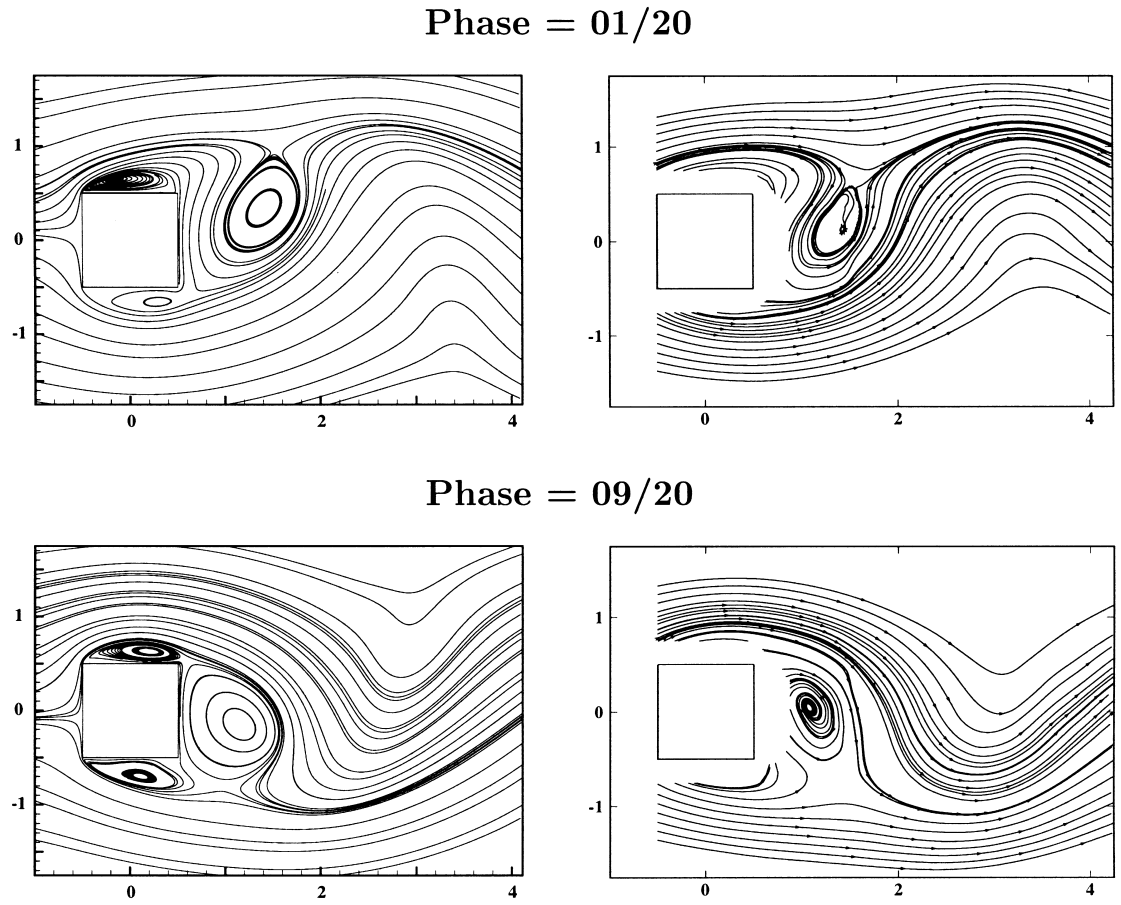

Fig. 8. Flow streamlines. Calculations (left) vs. measurements (right; from [3]. Computation with the SZL + AKN model.

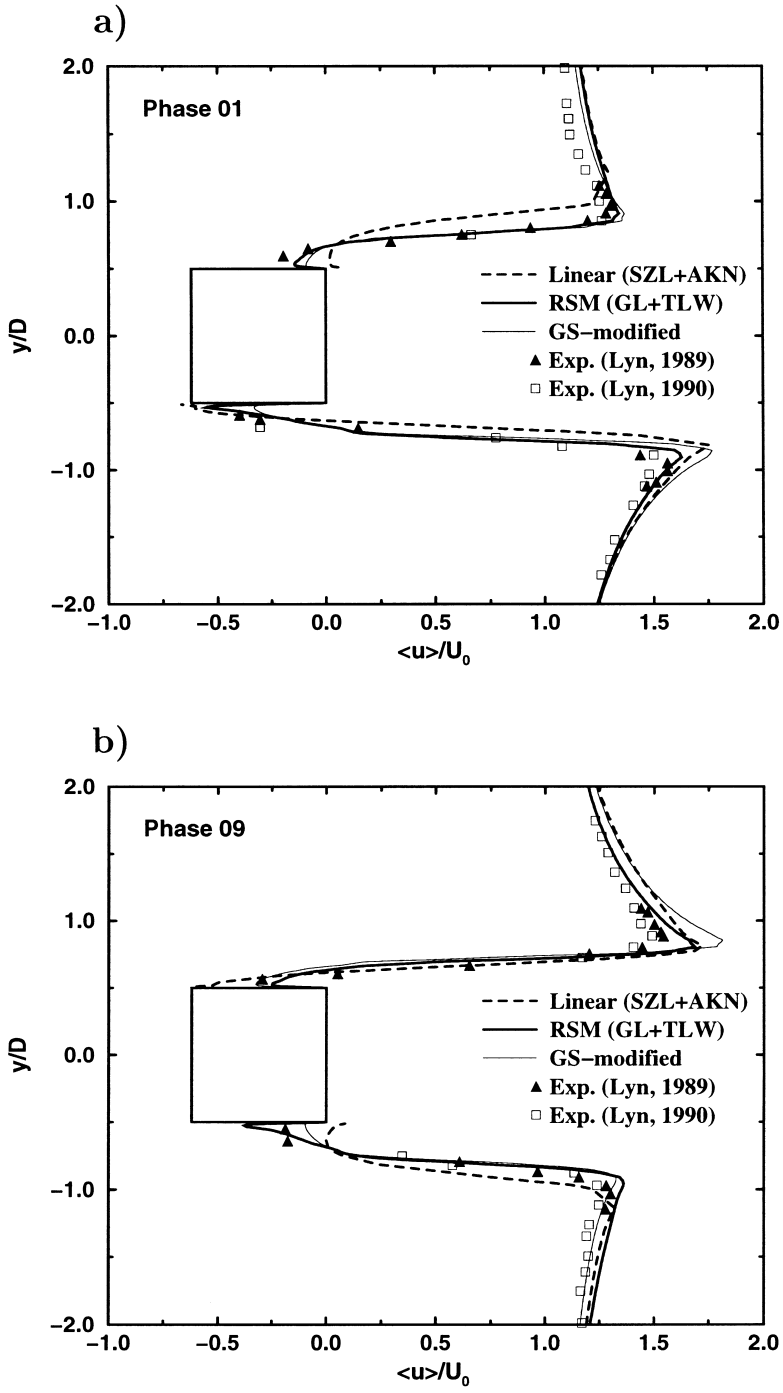

Fig. 9. Comparison of the phase-averaged streamwise velocity distribution at two phases: (a) phase 01/20; (b) 09/20.

quadratic or cubic. At this stage, it appears justifiable to reintroduce the Strouhal number St as an appropriate indicator of efficacy of the non-linear models, in contrast to conventional models, since previous investigations of the authors (results to be submitted) have revealed St to be much less sensitive to either the particular low-Re scheme utilized or to the imposed inflow conditions of turbulence.

The novel zonal Reynolds stress transport model is probably the most refined strategy for this particular flow. Results reported in Table 2 indicate a clear superiority in predicting mean drag coefficient $\bar{C}_d$ and recirculation length l_r, though the intensity of the wave motion, expressed through an overestimated St, is overpredicted. The present findings are in fact better than earlier results of Franke and Rodi [6]. Because the computation details are very similar (in particular, space and time differencing schemes, and time step Δt), the difference in behaviour stems probably from adopting the algebraic stress–strain relations in the one-equation model. In summary, the zonal RSM approach can produce much better global forces than selected LES (except Murakami's [10] contribution), which still display a disparate behaviour, at least in this particular context.

6.3. Phase-averaged quantities

Comparison of the phase-averaged quantities is limited here to flow streamlines Fig. 8, $\langle u \rangle$-velocity profiles in the leeward plane of the cylinder (Fig. 9), and $\langle v \rangle$-velocity profiles on the center line of the cylinder, calculated with the modified SZL and GS, and from the zonal RSM approach, respectively. The streamlines are compared with the experimental data of Lyn et al. [3], while selected data from earlier measurements of Lyn (private communications) are compared with the predicted $\langle u \rangle$- and $\langle v \rangle$-velocity profiles. The non-linear models produced virtually identical streamlines to that of the linear SZL model, and the same is true of the RSM. Clearly, there is reasonable agreement between computations and measurements, although there is a lack of information on the structure of attached/separated shear layers on side walls of the cylinder from the measurements. Close examination of Fig. 8 suggests, however, that the simulated shedding motion is more sustained than in the experiment, which conforms with the resulting integral parameters St and $\bar{C}_d$.

The superiority of both the modified GS model and the zonal RSM closure over the linear SZL model is reflected from the distributions of $\langle u \rangle$ velocity (Fig. 9), which indicate that EASMs and RSM only are able to adequately reproduce the reverse flow on both sides of the body simultaneously; this is a major improvement in comparison with the previous results of Franke and Rodi, including their two-layer, second-order LRR model. However, as has been so far aknowledged that an accurate prediction of the flow in this region is strongly dependent on the numerics rather than the turbulence modelling [11], establishing the superiority of one model over the other cannot be justified in this context. It should be mentioned here that no model has predicted flow reattachment on the side wall during the selected phases. Ensemble-averaged $\langle v \rangle$-velocity profiles plotted in Fig. 10 have the merit of revealing the strength of the shedding process in the wake. Indeed, far downstream of the cylinder (at $x/D > 4$), all the calculations predict the lateral ensemble-averaged velocity much higher than in experiment.

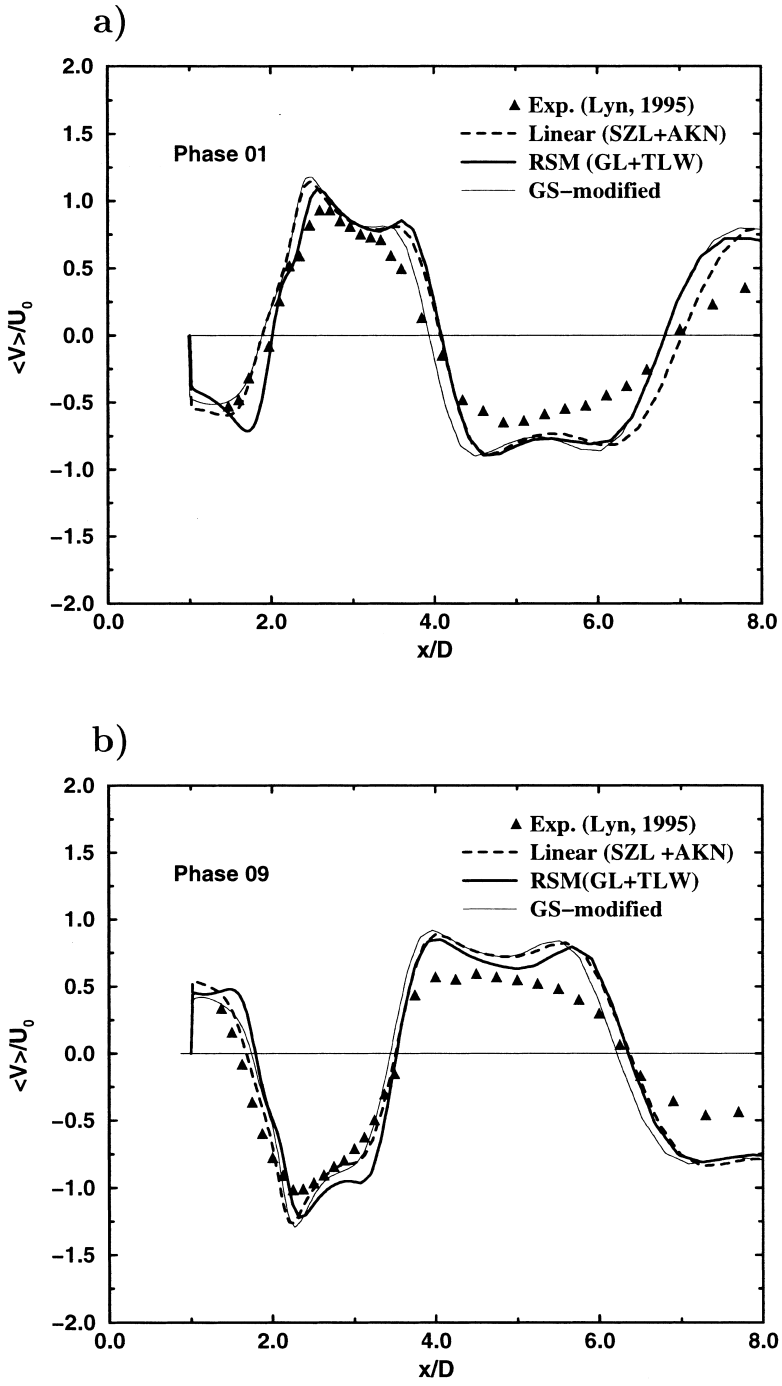

Fig. 10. Comparison of the phase-averaged vertical velocity distribution at two phases: (a) phase 01/20; (b) 09/20.

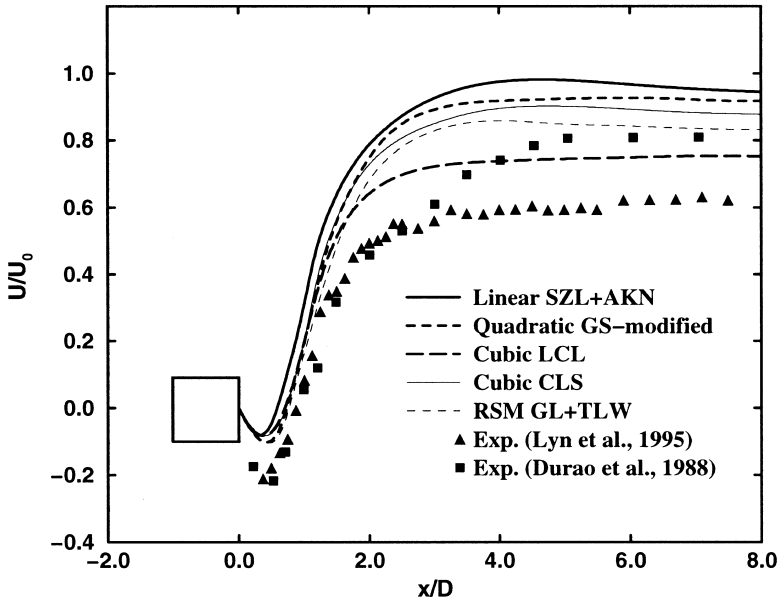

Fig. 11. Mean streamwise velocity distribution along the centre-line of the cylinder.

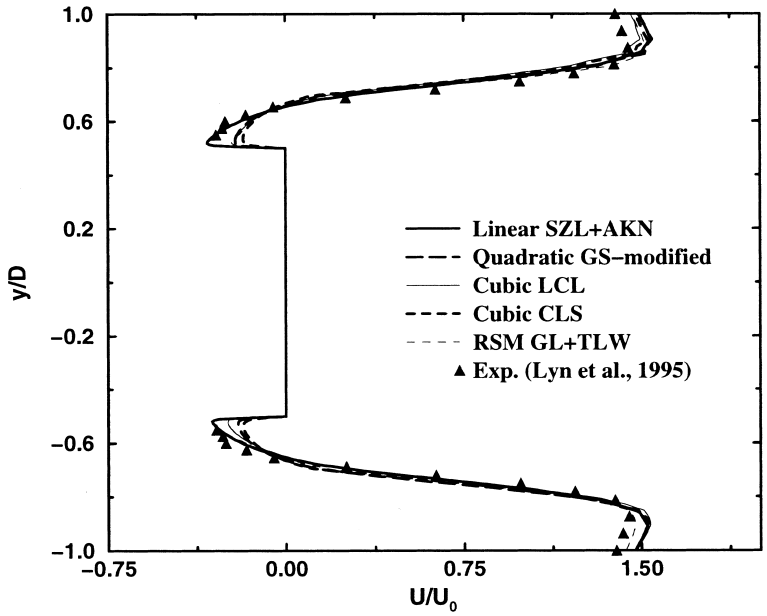

Fig. 12. Mean streamwise velocity distribution at the mid-plane of the cylinder; at location $x/D = 0.5$.

This shows the excessive rate of momentum exchange in the wake affects not only the shedding frequency and drag coefficient, but also the vertical velocity component.

6.4. Time-averaged quantities

Time-averaged streamwise velocities $\bar{U}$ along the centerline of the cylinder are compared for different cases in Fig. 11. The information concerning the length of the recirculation zone already discussed is confirmed: l_r is underestimated by the SZL model, while the non-linear models and the zonal RSM model show clear improvement. None of the models is able to correctly predict the backflow which is always underestimated. This result was formerly attributed by Deng et al. [8] to the smaller computational domain, whereas the recent analysis of freestream turbulence effects by the authors, has revealed that a high level of imposed effective viscosity significantly influences the backflow too. However, apart from the linear SZL model which, exhibits a very fast approach to the free-stream velocity due to an intensive shedding motion in body wake, there are large variations between all the other models. In all situations, flow recovery to the non-perturbed state is prematurely predicted, though less so for the cubic LCL and the zonal RSM, at least if the comparisons are limited with Durao' et al. [4] measurements. This behaviour arises as a common picture of two-dimensional RANS, as has been revealed by many authors (at least these cited here). Following Williamson [43] indeed, a nominally two-dimensional motion of the coherent structures engenders a transfer of kinetic energy towards the third direction. This feature cannot be captured by any sort of two-dimensional calculation.

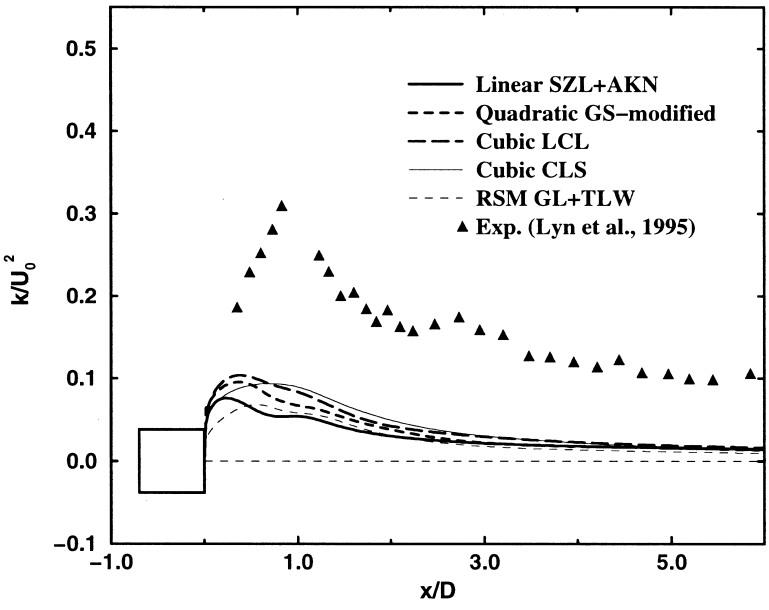

Fig. 13. Mean turbulent kinetic energy distribution on the centre-line of the cylinder.

Fig. 12 presents a close-up of the distribution of mean velocity $\bar{U}$ at the mid-plane of the cylinder. The mean flow field in this region is particularly well described by all models, and complete agreement with experiment is nearly achieved. This is the best guarantee of adequate grid resolution on the cylinder side-walls. The superior behaviour of the SZL model regarding prediction of the reverse flow very close to the wall is, as mentioned earlier, a possible consequence of over-suppression of turbulence production P_k at flow stagnation. Since this location is entirely dominated by shear, the impact of the non-linear terms in b_{ij} is minor, so that the efficiency of the model can be judged entirely with respect to C_μ. Such an observation was already noted by Lakehal and Rodi [38] when the Kato and Launder P_k-suppression measure [9] was employed for the flow past a 3D mounted-cube. As was to be expected, only marginal deviations between the EASMs and RSM results can be noticed in this narrow flow region adjacent to the wall.

The results of the mean turbulent kinetic-energy contribution to the total fluctuating one are compared with the experimental data in Fig. 13. Overall, the level of calculated turbulent kinetic energy is much too small, though a relative improvement (about 30% is now visible through the incorporation of the cubic terms due to Suga into the LCL and CLS models, in comparison with the linear and quadratic closures, SZL and GS-modified. This result is not surprising in view of what was originally expected from the additive cubic correlations of S_{ij} and Ω_{ij}, namely to enhance sensitivity to streamline curvature. More precisely, the two groups $C_6(T_{ij})_6$ and $C_7(T_{ij})_7$ constitute the unique linkage between anisotropy and shear stress through the quantity $(S^2 - \Omega^2)$, which is negative within the curved shear-layers bordering the Kármán street. Lien et al. [20] report about this feature in the wake of a flow past a 2D hill. Such a linkage may increase the effective viscosity through the corrected coefficient C_0, as explained previously, and explains the scatter in the profiles of k. However, there is really no clear indication on how important the sensitivity to streamline curvature in the wake flow region is exactly represented by these additive groups in (b_{ij}).

The enhanced level of turbulent kinetic energy in the wake by the cubic models might find its roots in the low-frequency fluctuations exhibited by the drag signals; a statement which is in line with the observations of Lyn et al. [3]. On the other hand, Williamson's [43] review on vortex dynamics in the cylinder wake states that the three-dimensionality of the coherent structures generates a secondary flow instability which, in turn, supplies the three-dimensional stochastic fluctuating field. In other words, a nominally two-dimensional vortex motion in the cylinder wake hides an intensive three-dimensionality of the non-coherent fluctuations. A purely second-order closure, together with a near-wall one-equation EASM, also fails to reproduce the rate of turbulent kinetic energy. Since this weakness is now acknowledged to be the logical consequence of forcing two-dimensionality on the flow, it is not evident to allow one to question the employed modelling strategies as a matter of priority.

Fig. 14a compares k_{tot}, the total fluctuating energy (periodic and turbulent) with measurements. The figure shows that, overall, reasonable agreement is achieved, though the peak is occasionally underpredicted. Significant departures of the values both from each other and from the data of Lyn are revealed in the far wake region, except from the LCL cubic model. Note, in addition, that nearly all models which overpredict k_{tot} in the energy-decay region systematically exaggerate both the mean drag coefficient and Strouhal number (see

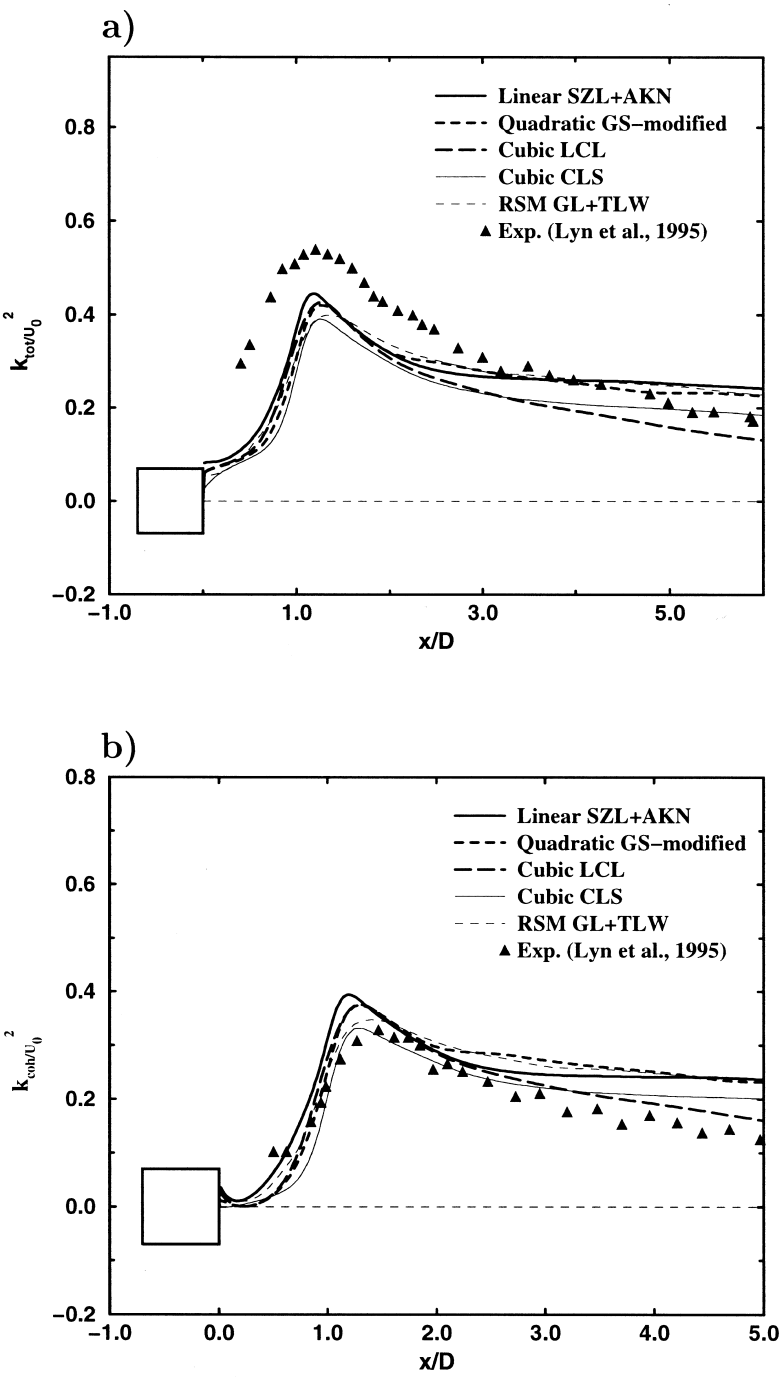

Fig. 14. Distribution of mean total fluctuating energy (a) and coherent fluctuating energy (b) along the centre-line of the cylinder.

Table 2). This scatter between the predictions reinforces the uncertainty regarding the behaviour of the selected stress–strain relationships in the wake region.

Franke and Rodi [6] obtained the best agreement with Lyn's data by employing the LRR second-order closure with wall functions, as compared with two-layer LRR calculations, which overpredicted k_{tot} by about 20%. In both cases, however, their RSM was found to severely overpredict the coherent fluctuating energy. In fact, except from Deng's et al. calculations, nearly all other methods referred to here fail to predict this quantity, including the recent LES calculations assembled by Rodi et al. [11], as well as previous ones performed by Murakami et al. [10]. The present zonal RSM approach predicts fairly well the level of wave-induced energy k_{coh} as shown in Fig. 14b, which is a major achievement with regard to the forgoing calculations. Both the level and location $x/D = 1.6$ of the coherent kinetic energy are well captured by the model. The cubic CLS model renders a much better agreement with the measurements of Lyn than all other EASMs. The peak in k_{coh} is, in particular, well predicted, and the same is true of k_{coh}-level in the energy-decay region. A close look at Fig. 14b suggests that k_{coh} is almost negligible in the backflow region (at $x/D < 0.5$), while Deng's results show a much too higher value there. This issue needs further analysis by LES, since none of the experiments has reported information concerning the distribution of k_{coh} in the close vicinity of the cylinder.

The mean pressure distributions around the cylinder, obtained from the different modelling procedures, are compared in Fig. 15 with the experimental data of Lee [44], and of Bearman and Obasaju [45]. Comparisons should in fact be made only with Lee's [44] data, since the

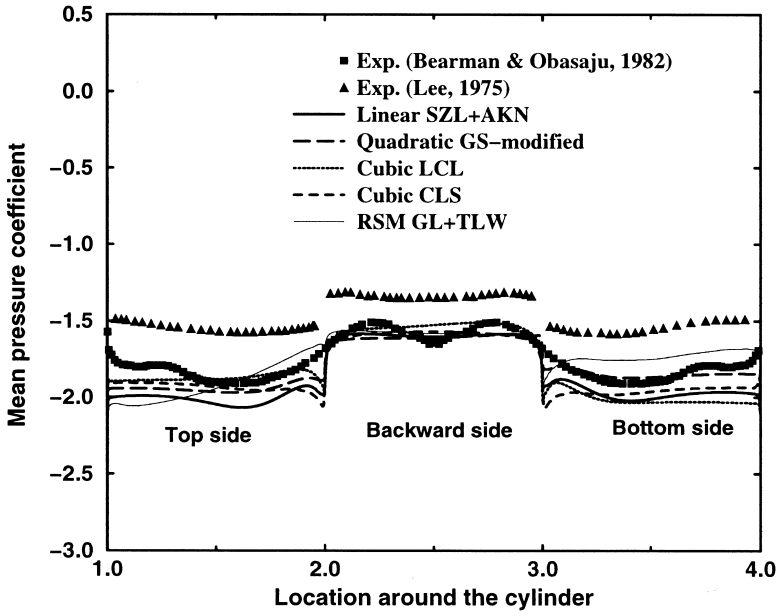

Fig. 15. Comparison of the mean pressure distribution around the cylinder.

freestream turbulence in Bearman and Obasaju's experiment was $< 0.04\%$, and their data were not corrected for blockage. Much better predictions of $\bar{C}_p$ on the backward face were obtained in comparison with Bearman and Obasaju' data than with those of Lee. On the side-walls of cylinder, however, it is evident that no clear picture of the two-equation models can be drawn, since all of them underpredict $\bar{C}_p$, although the EASMs deliver better results than the anisotropic SZL model. This result is entirely consistent with the forgoing remark, that is, two-equation models in general drive spurious momentum exchange in the wake, though less pronounced for the non-linear variants (LCL, GS and CLS). The zonal second-order closure behaves somewhat differently; in particular, for the asymmetric distribution of $\bar{C}_p$ on the cylinder side-walls, which is anyway in closer agreement with Lee's data than any other model. Admittedly, this distribution of $\bar{C}_p$ might have roots in the period doubling scenario shown in Fig. 6, but also in the asymmetric shedding about the wake centerline, as discussed previously. Note, also, that earlier RSM results of Franke and Rodi are even not comparable with the present SZL results, since the base pressure value was predicted too low. Supported by the global forces assembled in Table 2, the performance of the proposed RSM in predicting the pressure loads is within the accuracy of most of the selected LES reported by Rodi et al. [11] and Murakami et al. [10]. Still, the best agreement with Lee's [44] data have been obtained by simply performing laminar calculations or by employing the Baldwin–Lomax model [8]. Hence, a central question remains: why do nearly all LES and RANS predict the base pressure $\bar{C}_{p_b}$ systematically closer to Bearman and Obasaju's [45] data than to those of Lee [44]?

7. Concluding remarks

The vortex-shedding flow past a square cylinder at $Re = 22{,}000$ has been extensively investigated using different algebraic Reynolds stress closures, two of which being successfully modified to cope with flows undergoing large straining. A novel zonal modelling strategy combining a RSM for the outer core flow with a near-wall, one-equation ASM was successfully employed. The results of this strategy were found to be very encouraging, and to a large extent more accurate than those obtained by Franke and Rodi [6] using a similar methodology but adopting a linear, one-equation model near the wall. The improvement is due to the adoption of stress–strain relationships, based on the same pressure–strain model employed by the RSM for the outer core flow. This approach serves to smooth the discontinuities between the turbulent stresses in each layer. More interesting to note is the capability of the RSM methodology proposed here to capture the phenomenon of periodic doubling, in total accordance with the forgoing investigations based on DNS [40,41] and measurements [42] in which two-dimensionality of the flow was deliberately forced.

The modified anisotropic eddy viscosity SZL model, applied in linear form, produced good results, despite an overprediction of shedding frequency due to a strong reduction in turbulence production. This suggests that anisotropic eddy-viscosity models should be used in the context of full algebraic stress methodology. The comparison of both phase- and time-averaged velocity components obtained with the modified GS algebraic stress model showed very good agreement with the measurements. This represents a substantial improvement over the original

regularized proposal of Gatski and Speziale, which fails anyway to predict highly strained flows.

All the models considered in here, provide, however, a common picture: that is, the non-coherent fluctuating energy is grossly underpredicted, despite the visible improvement brought about by the inclusion of cubic terms in the anisotropic stress tensor b_{ij}. The total kinetic energy was, however, fairly-well predicted by all models, and the same is true of the wave-induced kinetic energy. To be pragmatic, one should acknowledge that the considered flow, being massively strained and having a laminar-turbulent transitional behaviour, poses great difficulties to idealized 2D modelling methodologies. These methods aim at forcing the motion of the coherent vortices to two-dimensionality, while this complex mechanism is known to generally oscillate between various three-dimensional modes, A and B [43], S [41]. Doing so, the significant effects of the non-linear interactions between these modes and their associated instabilities on the stochastic fluctuating field are systematically ignored.

The global parameters showed much better agreement with measurements than those obtained using LES (Table 2), including the recirculation length behind the body. However, overpredicting $\bar{C}_{\mathrm{d}}$, $\bar{C}_{\mathrm{l}}$ and St, i.e. the signature of intensive shedding dynamics, is presumably another consequence of forcing the mean flow to two-dimensionality. Recent direct numerical simulations [43] have clearly shown that a nominally two-dimensional shedding motion is associated with the redistribution of wave-induced kinetic energy in all directions, a feature which is simply out of reach of any 2D idealization. Therefore, while recognizing the potential of the LES concept, future research should also be aimed towards *Conditional Ensemble-Averaged Navier–Stokes Equations* applied in three-dimensions, of course, provided that the flow is dominated by a single shedding frequency.

Acknowledgements

Financial support was provided by the Deutsche Forschungs Gemeinshaft (DFG) within the framework of the French–German Collaborative Research programme Numerical Flow Simulation, while the first author was affiliated with TU-Berlin. The authors thank Dr. Brian Smith (PSI, Switzerland) who reviewed the manuscript. The computations were performed on the Cray T90 at the University of Kiel, Germany.

References

[1] Lakehal D. Computation of vortex shedding past bluff bodies employing statistical turbulence models, Internal Report: 02-1998, Hermann Föttinger Institut für Strömungsmechanik, Technical University of Berlin, 1998.

[2] Lakehal D, Thiele F, Duchamp DL, Buffat M. Computation of vortex-shedding flows past a square cylinder employing LES and RANS. In: Hirschel EH, editor. Notes on numerical fluid mechanics, vol. 66. Braunschweig: Vieweg Verlag, 1998. p. 260.

[3] Lyn DA, Einav S, Rodi W, Park JH. A laser-doppler velocimetry study of ensemble-averaged characteristics of the turbulent near wake of a square cylinder. Journal of Fluid Mechanics 1995;304:285.

[4] Durao DFG, Heitor MV, Pereira JCF. Measurements of turbulent and periodic flows around a square cross section cylinder. Experiments in Fluids 1988;6:298.
[5] Bosch G. Experimentelle und theoretische Untersuchung der instationären Strömung um zylindrische Strukturen, Ph.D Thesis, University of Karlsruhe, 1995.
[6] Franke R, Rodi W. Calculation of vortex shedding past a square cylinder with various turbulence models. In: Durst F, et al., editors. Turbulent shear flows, vol. 8. Berlin: Springer, 1993.
[7] Kawamura H, Kawashima N. An application of a near wall $k-\tilde{\varepsilon}$ model to the turbulent channel flow with transpiration and to the oscillatory flow around a square cylinder. Symposium Turbulence, Heat and Mass Transfer 2, Delft, 1997.
[8] Deng DW, Piquet J, Queutey P, Visonneau M. 2D computations of unsteady-flow past a square cylinder with the Baldwin–Lomax model. Journal of Fluids and Structures 1994;8(7):663.
[9] Kato M, Launder BE. The modeling of turbulent flow around stationary and vibrating square cylinders. In: Proceedings Turbulent Shear Flows 9 (10-4-1), Kyoto. 1993.
[10] Murakami S, Mochida A. On turbulent vortex shedding flow past 2D square cylinder predicted by CFD. Journal of Wind Engineering Industrial Aerodynamics 1995;54/55:191.
[11] Rodi W, Ferziger J, Breuer M, Pourquier M. Status of large eddy simulation. Results of a workshop. ASME Journal of Fluids Engineering 1997;119:248.
[12] Yu D, Kareem A. Numerical simulation of flow around rectangular prism. Journal of Wind Engineering Industrial Aerodynamics 1997;67:197.
[13] Reynolds WC, Hussein AKMF. The mechanisms of an organized wave in turbulent shear flow. Part 3: Theoretical models and comparisons with experiments. Journal of Fluid Mechanics 1972;54:263.
[14] Jones WP, Launder BE. Prediction of relaminarization with a two-equation turbulence model. International Journal Heat Mass Transfer 1972;15:301.
[15] Rodi W. A new algebraic relation for calculating the Reynolds stresses . ZAMM 1976;56:T219.
[16] Gatski TB, Speziale CG. On explicit algebraic stress models for complex turbulent flows. Journal of Fluid Mechanics 1993;254:59.
[17] Pope SG. A more general effective viscosity hypothesis. Journal of Fluid Mechanics 1975;72:331.
[18] Suga K. Development and application of a non-linear eddy-viscosity model sensitized to stress and strain invariants. PhD dissertation, Department of Mechanical Engineering, UMIST, 1995.
[19] Craft TJ, Launder BE, Suga K. Development and application of a cubic eddy-viscosity model of turbulence. International Journal Heat and Fluid Flow 1996;17:108.
[20] Lien FS, Chen WL, Leschziner MA. low-*Re*ynolds-number eddy-viscosity modelling based on non-linear stress–strain/vorticity relations. In: Proceedings Third International Symposium of Engineering Turbulence Modeling and Measurements, Creta, Greece. 1996.
[21] Speziale CG, Sarkar S, Gatski TB. Modelling the pressure–strain correlation of turbulence: an invariant dynamical systems approach. Journal of Fluid Mechanics 1991;227:245.
[22] Speziale CG. Turbulence modelling for time dependent RANS and VLES: a review. AIAA Journal 1998;36(2):173.
[23] Grimaji S. Fully explicit and self-consistent algebraic reynolds stress model. Theoretical and Computational of Fluid Dynamics 1996;8:387.
[24] Jongen T, Gatski TB. A new approach to characterizing the equilibrium states of the Reynolds stress anisotropy in homogeneous turbulence. Theoritical and Computational Fluid Dynamics 1998;11:31.
[25] Laufer J. Investigation of turbulent flow in a two-dimensional channel, NACA TN 1053, 1951.
[26] Speziale CG, Mac Giolla Mhuiris N. On the prediction of equilibrium states in homogeneous turbulence. Journal of Fluids Mechanics 1989;209:591.
[27] Kim J, Moin P, Moser R. Turbulent statistics in fully developed channel flow at low Reynolds number. Journal of Fluid Mechanics 1987;177:133.
[28] Lee MJ, Kim J, Moin P. Structure of turbulence at high shear rate. Journal of Fluid Mechanics 1990;216:51.
[29] Rogers MM, Moin P. The structure of vorticity field in homogeneous turbulent flows. Journal of Fluid Mechanics 1990;176:33.
[30] Norris LH, Reynolds WC. Turbulent channel flow with a moving wavy boundary. Rept. No. FM-10, Stanford University, Department of Mechanical Engineering, 1975.

[31] Shih TH, Zhu J, Lumley JL. A new reynolds stress algebraic equation model. Computer Methods in Applied Mechanics and Engineering 1995;125:287.
[32] Abe K, Kondoh T, Nagano Y. A new turbulence model for predicting fluid flow and heat transfer in separating and reattaching flows. Part I: Flow field calculations. International Journal of Heat Mass Transfer 1994;37(1):139.
[33] Launder BE, Reece G, Rodi W. Progress in the development of a Reynolds stress turbulence closure. Journal of Fluid Mechanics 1975;68:537.
[34] Wolfshtein M. The velocity and temperature distribution in one-dimensional flow with turbulence augmentation and pressure gradient. International Journal of Heat Mass Transfer 1969;12:301.
[35] Daly BJ, Harlow FH. Transport equations in turbulence. Physics of Fluids 1970;13(11):2634.
[36] Gibson MM, Launder BE. The effects on pressure fluctuations in the atmospheric boundary layer. Journal Fluid Mechanics 1978;86:491.
[37] Gibson MM, Younis BA. Calculation of swirling jets with a Reynolds stress closure. Physics of Fluids 1986;29(1):38.
[38] Lakehal D, Rodi W. Calculation of the flow past a surface-mounted cube with two-layer turbulence models. Journal of Wind Engineering and Industrial Aerodynamics 1997;67-68:65.
[39] Karniadakis GE, Triantafyllou GS. Three-dimensional dynamics and transition to turbulence in the wake of bluff objects. Journal of Fluids Mechanics 1992;238:1.
[40] Sohankar A, Norberg C, Davidson L. Simulation of three-dimensional flow around a square cylinder at moderate Reynolds number. Physics of Fluids 1999;11(3):288.
[41] Robichaux J, Blachandar S, Vanka SP. Three-dimensional floquet instability of the wake of square cylinder. Physics of Fluids 1999;11(3):560.
[42] Henderson RD. Nonlinear dynamics and pattern formation in turbulent wake transition. Journal of Fluids Mechanics 1997;352:65.
[43] Williamson CHK. Vortex dynamics in the cylinder wake. Annual Review Fluid Mechanics 1996;28:477.
[44] Lee BE. The effect of turbulence on the surface pressure field of square. Prisms Journal of Fluid Mechanics 1975;69:263.
[45] Bearman PW, Obasaju ED. An experimental study of pressure fluctuations on fixed and oscillating square section cylinders. Journal of Fluid Mechanics 1982;119:297.